Glycoproteome remodelling and granule-specific *N*-glycosylation accompany neutrophil granulopoiesis

Rebeca Kawahara[1^], Julian Ugonotti[1^], Sayantani Chatterjee[1], Harry C. Tjondro[1], Ian Loke[2], Benjamin L. Parker[3], Vignesh Venkatakrishnan[4,5], Regis Dieckmann[4], Zeynep Sumer-Bayraktar[1], Anna Karlsson-Bengtsson[4,5], Johan Bylund[6], Morten Thaysen-Andersen[1,7]*

[1]School of Natural Sciences, Macquarie University, Sydney, New South Wales 2109, Australia
[2]Cordlife Group Limited, Singapore 768160, Singapore
[3]Department of Anatomy and Physiology, University of Melbourne, Melbourne, Victoria 3010, Australia
[4]Department of Rheumatology and Inflammation Research, Institute of Medicine, Sahlgrenska Academy, University of Gothenburg, Gothenburg, Sweden
[5]Department of Life Sciences, Chalmers University of Technology, Gothenburg, Sweden
[6]Department of Oral Microbiology and Immunology, Institute of Odontology, Sahlgrenska Academy, University of Gothenburg, Gothenburg, Sweden
[7]Institute for Glyco-core Research (iGCORE), Nagoya University, Nagoya, 464-8601, Japan

[^]These authors contributed equally

Running title: Spatiotemporal glycoproteome remodelling in neutrophils

*Corresponding author
Associate Professor Morten Thaysen-Andersen, PhD
School of Natural Sciences
Macquarie University
NSW-2109, Sydney, Australia
Phone: +61 2 9850 7487 / Email: morten.andersen@mq.edu.au

Summary

Neutrophils store microbicidal glycoproteins in cytosolic granules to fight intruding pathogens, but their granule distribution and formation mechanism(s) during granulopoiesis remain unmapped. Herein, we perform comprehensive spatiotemporal *N*-glycoproteome profiling of isolated granule populations from blood-derived neutrophils and during their maturation from bone marrow-derived progenitors using glycomics-assisted glycoproteomics. Interestingly, the granules of resting neutrophils exhibited distinctive glycophenotypes including, most strikingly, peculiar highly truncated *N*-glycosylation in the azurophilic granules. Excitingly, proteomics and transcriptomics data from discrete myeloid progenitor stages revealed that profound glycoproteome remodelling underpins the promyelocytic-to-metamyelocyte transition and that remodelling is driven primarily by changes in protein expression and less by the glycosylation machinery. Notable exceptions were the oligosaccharyltransferase subunits responsible for initiation of *N*-glycoprotein biosynthesis that were strongly expressed in early myeloid progenitors correlating with high glycosylation efficiencies of the azurophilic granule proteins. Our study provides spatiotemporal insights into the complex neutrophil *N*-glycoproteome featuring an intriguing granule-specific *N*-glycosylation formed by dynamic remodelling during myeloid progenitor-to-neutrophil maturation.

Keywords: Granulopoiesis, neutrophil, metamorphosis, granule, myeloid progenitor, maturation, glycoproteome, remodelling, glycomics, glycoproteomics

Introduction

Neutrophils are critical first-line responders to infection and form a potent line of innate immune defence against invading pathogens[1,2]. Circulating in their resting state in blood, neutrophils are equipped with an arsenal of prepacked cytosolic granules[3]. The carefully timed mobilisation of these intracellular granules released upon specific environmental cues enables neutrophils to extravasate and traffic to inflammatory sites to elicit an effective, timely and well-balanced response against invading pathogens, which they fight by means of phagocytosis, degranulation and neutrophil extracellular traps[3,4].

Distinctly different granule populations are formed during the week-long maturation of neutrophils (granulopoiesis) in the bone marrow[3,5]. The azurophil granules (Az, or primary granules) are formed during the early myeloblast-to-promyelocyte (MB-to-PM) maturation stages whilst the specific granules (Sp, or secondary granules) are formed during the PM-to-myelocyte/metamyelocyte (MC/MM) stages. Finally, the gelatinase granules (Ge, or tertiary granules) form during the late MM-to-band cell (BC) maturation stages. Secretory (Se) vesicles, although not considered granules *per se*, form another type of membrane-enclosed intracellular compartments within neutrophils that arise from endocytosis of the plasma membrane during the final BC-to-mature neutrophil maturation stage[3]. Now well documented, the granule populations harbour distinct proteome signatures; the temporal granule formation during granulopoiesis is, through a mechanism known as 'targeting by timing', a recognised contributor to the granule-specific protein repertoires found in neutrophils[6,7].

Protein *N*-glycosylation, the covalent attachment of *N*-glycans to motif-restricted asparagine residues (Asn-X-Ser/Thr, X ≠ Pro), adds important structural and functional heterogeneity to proteins. Both the neutrophil cell surface and granule-resident glycoproteins are richly decorated with *N*-glycans that directly facilitate and more indirectly modulate key immune and

trafficking functions of neutrophils[4]. For example, neutrophil proteins are known to carry *N*-glycans containing Lewis X (Le^x) and sialyl-Lewis X (sLe^x) glycoepitopes[8], which interact with endothelial P- and E-selectins to mediate neutrophil tethering, rolling and extravasation to peripheral tissues[9,10].

Following our discovery of paucimannosidic *N*-glycans ($Man_{1-3}GlcNAc_2Fuc_{0-1}$) in the neutrophil-rich sputum from cystic fibrosis-affected individuals[11,12], we and others have demonstrated that neutrophils abundantly express paucimannose carried by Az granule-resident glycoproteins[12-14]. This was corroborated by several targeted glycoprofiling studies of specific neutrophil glycoproteins including cathepsin G (CTSG, UniProtKB P08311), neutrophil elastase (ELANE, P08246), and myeloperoxidase (MPO, P05164), known to reside primarily in the Az granules[15-18]. In further support, we recently demonstrated that human neutrophils generate paucimannose-modified proteins via a non-canonical *N*-acetylhexosaminidase (Hex)-mediated truncation pathway particularly active in the Az granules[19]. While well studied in plants and insects, the biological roles of paucimannosidic proteins in human neutrophils, however, remain poorly understood despite emerging evidence pointing to their involvement in key innate immune processes[20,21].

To better understand the complexity of neutrophil granule *N*-glycosylation, we recently performed *N*-glycome profiling of whole granules isolated from human neutrophils[14]. In line with our previous findings[12], glycome differences were consistently observed between granules. However, since glycomics does not provide site and protein carrier information critically important to understand neutrophil glycobiology and structure-function relationships of the microbicidal glycoproteins found in neutrophil granules, these details were left undocumented in that study. Complementing our approach, Reiding *et al*. used *N*-glycopeptide mapping of human neutrophils to study the identity of the neutrophil glycoproteins and their

glycosylation sites[13]. By mapping observed glycoproteins to pre-established granule libraries[7,22,23], the authors could infer glycosylation patterns related to different granule populations albeit without direct evidence of their spatial distribution.

We here set out to comprehensively profile the dynamic and complex neutrophil *N*-glycoproteome with spatial (granule) and temporal (maturation stage) resolution focusing specifically on characterising the luminal (soluble) granule fractions hosting most microbicidal glycoproteins. Using glycomics-assisted glycoproteomics of isolated granules from blood neutrophils complemented with multi-omics data interrogation of developing myeloid progenitors undergoing metamorphosis in the bone marrow, we here provide spatiotemporal insights into previously unknown neutrophil *N*-glycosylation processes. We find that the neutrophil *N*-glycoproteome exhibits fascinating site-, protein- and granule-specific *N*-glycosylation features and undergoes profound remodelling during the early stages of neutrophil maturation in the bone marrow.

Results

Spatiotemporal glycoproteome profiling of resting and maturing neutrophils

While protein glycosylation is widely recognised to shape and even define neutrophil function[4], the spatial *N*-glycoproteome distribution in neutrophil granules and the dynamic glycoproteome changes (remodelling) that may accompany the dramatic metamorphosis associated with the differentiation of myeloid progenitor cells to mature polymorphonuclear blood cells remain unknown. To this end, we firstly performed spatial *N*-glycoproteome profiling of resting neutrophils by applying integrated glycomics-assisted glycoproteomics[24,25] to isolated granule populations (**Figure 1A**). The temporal *N*-glycoproteome remodelling accompanying granulopoiesis was then explored by interrogating robust proteomics and transcriptomics resources generated from discrete myeloid progenitor subsets[26,27] for previously overlooked glycopeptide and glyco-enzyme expression patterns (**Figure 1B**).

The separation of the four major granule populations of neutrophils was guided by established immunoblot and enzyme activity assays against known granule markers across a spectrum of Percoll density fractions[14,28]. The granule separation was orthogonally validated using our acquired proteomics data by plotting the expression profile of protein markers known to be enriched in each granule including MPO in azurophilic granules (Az), lactoferrin (LTF, P02788) in specific granules (Sp), matrix metalloproteinase-9 (MMP9, P14780) in gelatinase granules (Ge) and ficolin-1 (FCN1, O00602) in a combined secretory vesicle/plasma membrane fraction (Se) (**Figure 1C**). Further supporting the precision of the granule separation, concordance was observed between our granule proteomics data and a landmark study also performing quantitative proteomics on separated neutrophil granules[7] as illustrated by high correlation (R = 0.886) of proteins identified in the Az granules (**Figure 1D**) and in other granules (Sp: R = 0.854; Ge: R = 0.610; Se: R = 0.890) (**Supplementary Table S1**).

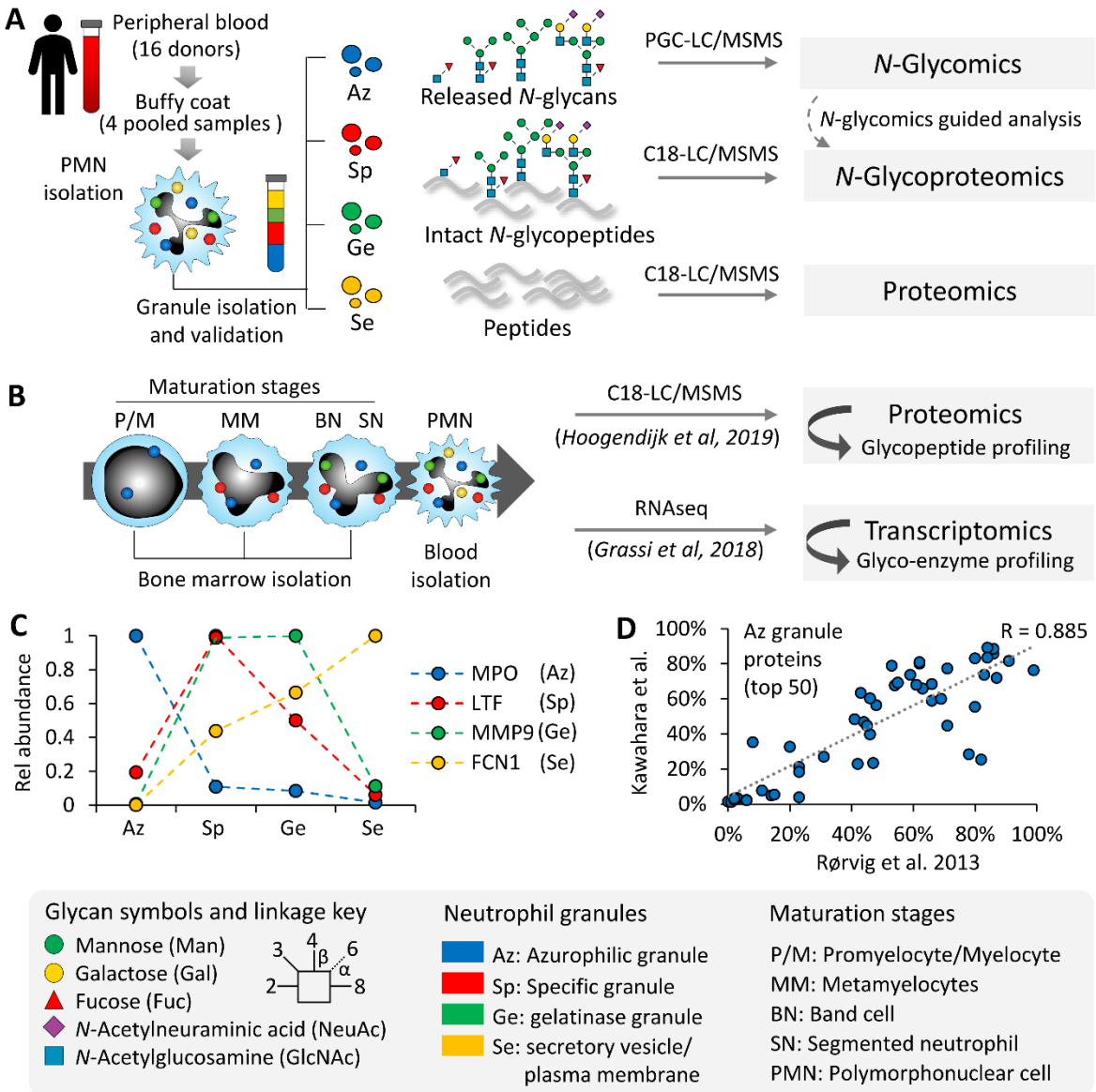

Figure 1. Spatiotemporal *N*-glycoproteome profiling of neutrophil granules and myeloid maturation stages using systems glycobiology approaches. A) Spatial *N*-glycoproteome profiling using quantitative glycomics-assisted glycoproteomics of the four major granule populations isolated from resting neutrophils. **B)** Temporal profiling of the *N*-glycoproteome and the underpinning glycosylation machinery of discrete neutrophil maturation stages from bone marrow-derived myeloid progenitor cells through interrogation of available proteomics and transcriptomics resources[26,27]. Neutrophil granule isolation was orthogonally validated using the generated proteomics data by **C)** plotting the expression profile of known neutrophil granule markers i.e. myeloperoxidase (MPO) for azurophilic granules (Az), lactoferrin (LTF)

for specific granules (Sp), matrix metalloproteinase-9 (MMP9) for gelatinase granules (Ge) and ficolin-1 (FCN1) for the secretory vesicles/plasma membrane (Se) and **D)** concordance of the 50 most abundant proteins identified in the Az granules against a key reference study also performing quantitative proteomics of separated neutrophil granules[7]. See **Supplementary Table S1** for the correlation of other granule datasets. See insert for key to the glycan symbols, linkage nomenclature and the neutrophil granules and maturation stages.

Distinct *N*-glycome signatures across the neutrophil granules

Firstly, deep quantitative glycomics performed using PGC-LC-MS/MS revealed a total of 71 protein-linked *N*-glycan structures spanning 43 *N*-glycan compositions across the neutrophil granules (**Supplementary Table S2**). PGC-LC-MS/MS-based glycomics is a particularly informative approach as it provides comprehensive evidence (LC retention time, molecular mass and fragmentation patterns) to determine key fine structural elements of glycans, including their topology (connectivity/branch points), terminal features (sialyl linkages, fucose position) and relative abundance, even in complex mixtures such as those from the neutrophil granules (see **Supplementary Data S1** for structural support of reported *N*-glycans).

Principal component analysis (PCA) of the *N*-glycomics data indicated that the neutrophil granule populations carry distinct *N*-glycome signatures (**Figure 2A**). The Az granules appeared particularly well separated from the other granule populations. With respect to the *N*-glycan type distribution, the Az granules displayed abundant paucimannosylation (~55%), with a single characteristic paucimannosidic *N*-glycan ($Man_2GlcNAc_2Fuc_1$) alone covering ~35% of the total Az *N*-glycome (**Figure 2B**). The Sp granules displayed mainly sialofucosylated complex-type *N*-glycans (~75%) while oligomannosidic- and less decorated complex-type structures were characteristic *N*-glycan types of both the Ge and Se granules.

Profound granule differences were also observed for the fine structural elements of the complex-type *N*-glycans. While core fucosylation (α1,6-fucosylation) was a prevalent feature across all granules, the Sp, Ge and Se compartments exhibited significantly lower core fucosylation (~45-70%) compared to the Az granules (~80%, all $p < 0.0001$, ANOVA test) (**Figure 2C**). In contrast, antenna fucosylation forming key Lewis-type glycoepitopes was near-absent in the Az granules (~3%) while being prominent features in other granules (~20-40%, all $p < 0.0001$, ANOVA test). Interestingly, sialyl linkage switching was also observed across the granules; the Az granules exhibited less α2,6-sialylation and high α2,3-sialylation relative to the Sp, Ge and Se granules (all $p < 0.01$ except for Az vs Se α2,3-sialylation, ANOVA test). Albeit of generally low abundance (0.5-1% of *N*-glycome), mannose-6-phosphate (M6P) containing oligomannosidic *N*-glycans (M6-M7) were additionally found to be elevated in the Ge and Se granules relative to the Az and Sp granules ($p < 0.01$, student's t-test) (**Figure 2D**). Lastly, dramatic differences in the antennary branching pattern were observed across the granules; unusual monoantennary complex-type *N*-glycans were features of the Az granules contrasting the bi-, tri- and higher branching in the Sp, Ge and Se granules (all $p < 0.0001$, ANOVA test) (**Figure 2E**). Granule-specific differences were also observed for these *N*-glycan features (fucosylation, sialylation, M6P, antennary branching) when measured as a proportion of identified structures having the potential to be modified by the specific glyco-feature rather than against the total *N*-glycome, a more appropriate measure when exploring biosynthetic relationships to observed *N*-glycome differences (**Supplementary Figure S1A-B**).

Recapitulating the granule-specific *N*-glycome differences, unsupervised clustering analysis of the glycomics data indicated four major glycan clusters (cluster 1-4), one for each granule type, and revealed individual *N*-glycan structures contributing to the granule differences (**Figure 2D,** see dendrogram in **Supplementary Figure S1C**). In short, cluster 1 (Az granules) were rich in

peculiar chitobiose core-, paucimannosidic- and monoantennary complex-type *N*-glycans, cluster 2 (Sp granules) featured highly sialylated and core/antenna fucosylated complex-type branched *N*-glycans, cluster 3 (Ge granules) exhibited M6P-oligomannosylation, and cluster 4 (Se granules) oligomannose and less sialofucosylated complex-type *N*-glycans. Taken together, our comprehensive *N*-glycome map of luminal (soluble) proteins from the neutrophil granules, the most detailed to date, demonstrates prominent granule-specific *N*-glycan differences across the neutrophil granules.

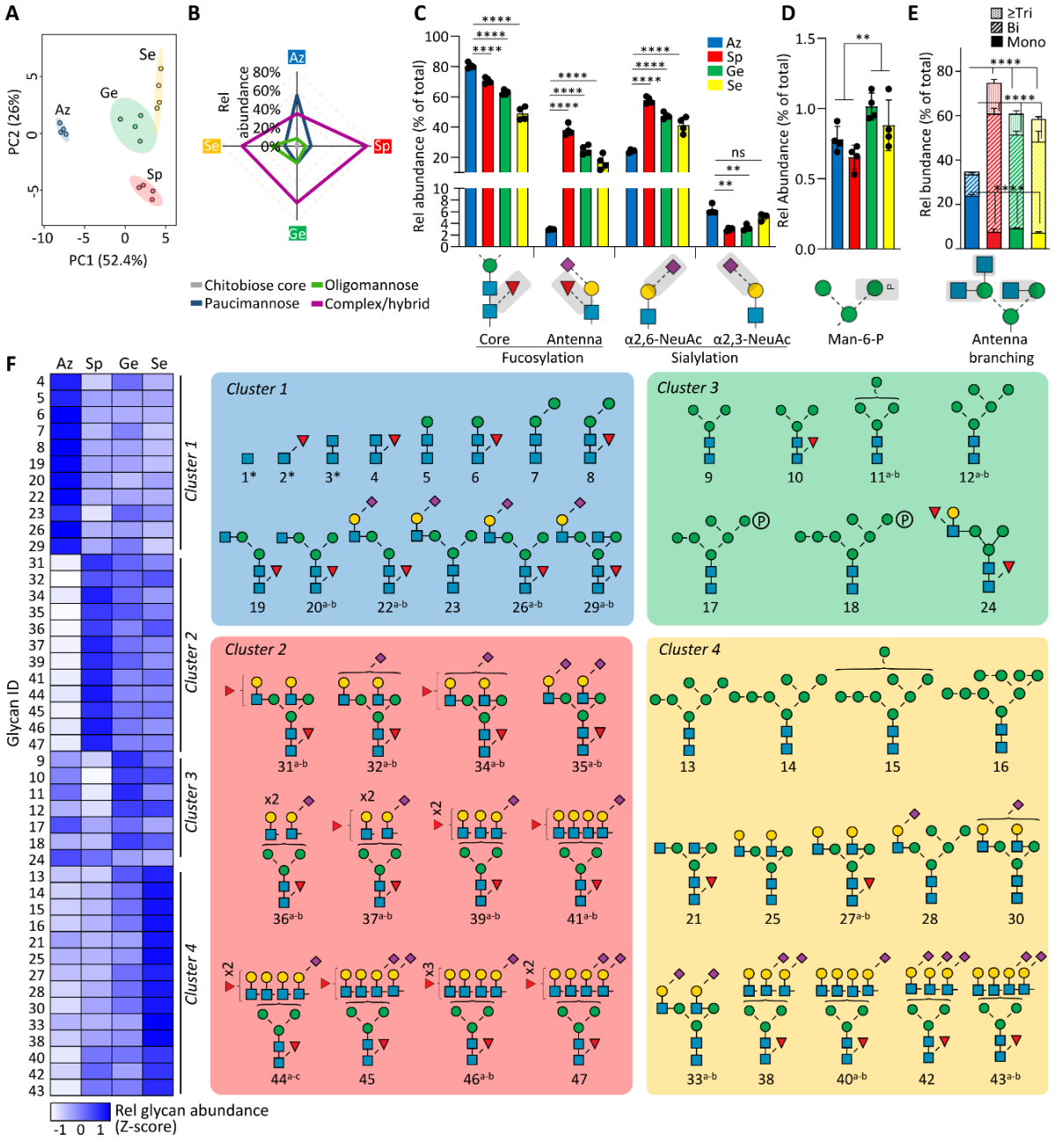

Figure 2. Granule-specific *N*-glycome signatures in resting neutrophils. A) PCA of quantitative *N*-glycomics data of the four granule populations (Az, Sp, Ge, Se) isolated from resting neutrophils. **B)** *N*-glycan class distribution across granules. Key glyco-features across granules including **C)** core/antenna fucosylation and α2,3-/α2,6-sialylation, **D)** mannose-6-phosphate (M6P) modifications and **E)** antennary branching patterns (relative abundance of each glyco-feature against the total *N*-glycome). For panel B-E, data plotted as mean and SD (n = 4 biological replicates, SD left out in panel B for simplicity, ANOVA test, $^{**}p < 0.01$, $^{****}p < 0.0001$, ns, not significant). **F)** Left: Unsupervised clustering (see **Supplementary Figure S1C** for dendrogram) and heatmap of *N*-glycomics data illustrating four major clusters representing the neutrophil granule populations. Right: *N*-glycan structures contributing to each cluster. The most common structure is depicted for glycan compositions exhibiting multiple isomers. *chitobiose core-type *N*-glycans reported at the glycopeptide level. See Figure 1 for key. See **Supplementary Table S2** for glycan identifiers consistently used throughout the study.

Glycoproteomics reveals granule-, protein- and site-specific *N*-glycosylation in neutrophils

Robust *N*-glycoproteomics data were obtained from the neutrophil granules using high resolution LC-MS/MS of peptide mixtures with and without *N*-glycopeptide enrichment. Data were searched for intact *N*-glycopeptides using a tailored glycan database comprising only *N*-glycans already identified by glycomics. Glycomics-guided glycoproteomics[24,25] is beneficial as it reduces the glycopeptide mis-identification (false-discovery rate) and search time, two recognised bottlenecks in glycoproteomics data analysis[29], while it, in parallel, provides quantitative structural details of the *N*-glycans in the *N*-glycoproteome as presented above.

Collectively, a total of 27,663 *N*-glycoPSMs from 4,772 unique *N*-glycopeptides (unique protein, site and glycan) spanning 627 *N*-glycosites and mapping to 352 source *N*-glycoproteins

were identified across the neutrophil granules (**Supplementary Figure S2A** and **Supplementary Table S3**). Despite using highly conservative confidence thresholds to ensure accurate glycopeptide identification (FDR < 1%, manual curation, bespoke glycan database i.e. 47 *N*-glycan compositions observed with glycomics), our analysis provides the, to date, deepest coverage of the neutrophil *N*-glycoproteome, greatly expanding on findings from a recent neutrophil glycoproteomics study performed without granule fractionation and using a large glycan database (279 *N*-glycan compositions) for data searching[13] (**Supplementary Figure S2B-C**). Our glycomics-informed glycoproteomics approach therefore facilitated both an extensive glycoproteome coverage, and, importantly, an accurate and unbiased view of the neutrophil *N*-glycoproteome as supported by consistent correlations between our glycomics and glycoproteomics data across granules (Az: R = 0.588, Sp: R = 0.505, Ge: R = 0.529, Se: R = 0.419, **Supplementary Figure S3A-B**). Importantly, the glycopeptides identified in the enriched and unenriched fractions showed a similar glycan distribution (Az: R = 0.875, Sp: R = 0.649, Ge: R = 0.789, Se: R = 0.906), supporting that both sample types enable unbiased *N*-glycoproteome profiling of the neutrophil granules (**Supplementary Figure S3C-D**).

Interestingly, the glycopeptide spectral prevalence in the Az granules (averaging 2,558 *N*-glycoPSMs/run) far outnumbered the glycopeptide spectral count in other granules (700-1,501 *N*-glycoPSMs/run) (**Figure 3A**). Despite the higher proportion of glycopeptide spectra in the Az datasets, a similar number of unique glycopeptides but mapping to less source *N*-glycoproteins (94 proteins) were observed for the Az granules relative to the other three granule populations (139-199 proteins/granule type), suggesting a higher glycan density per protein and, therefore, a higher occupancy of the available glycosylation sites (effectively a higher 'glycosylation efficiency') of the proteins residing in the Az granules.

PCA of the glycoproteomics data recapitulated the glycomics-informed separation of the four granule populations supporting their distinctive glycophenotypes and highlighted again the

unique glycosylation features of the Az granules (**Figure 3B**). In line with the glycomics data, the glycoproteomics data indeed showed that the Az granules exhibit higher levels of chitobiose core- and paucimannosidic-type *N*-glycans and concomitant lower levels of oligomannosidic- and complex-type *N*-glycans relative to the Sp, Ge and Se granules (**Figure 3C**).

The information-rich glycoproteomics data revealed a profound microheterogeneity featuring an extensive diversity and variation of the *N*-glycan distribution across sites and proteins as illustrated for the eight most abundant glycoproteins (of a total of 100-200 glycoproteins per granule) in each granule (**Figure 3D**). As an example of the profound site- and protein-specific *N*-glycosylation and in general agreement with recent literature[12,17], the six *N*-glycosites of the Az-resident MPO were found to carry different *N*-glycosylation distribution patterns (N139: complex-type, N355/N391: oligomannosidic-type, N323/N483/N729: paucimannosidic-type) that were distinctly different to other Az glycoproteins including the chitobiose core-rich CTSG (see **Supplementary Table S4** for all *N*-glycopeptides profiled in the neutrophil granules). Importantly, while each glycoprotein (and each site) exhibited a distinctive glycosylation distribution pattern, the granule-specific *N*-glycosylation features documented by glycomics were recapitulated in the glycoproteomics data as illustrated by similar glycan-based clustering patterns across granules (**Supplementary Figure S4**).

Taken together, our comprehensive glycomics-assisted glycoproteomics analysis of the four major granule populations isolated from resting neutrophils provides deep spatial insight into the complex neutrophil *N*-glycoproteome that exhibits fascinating granule-, protein- and site-specific *N*-glycosylation features.

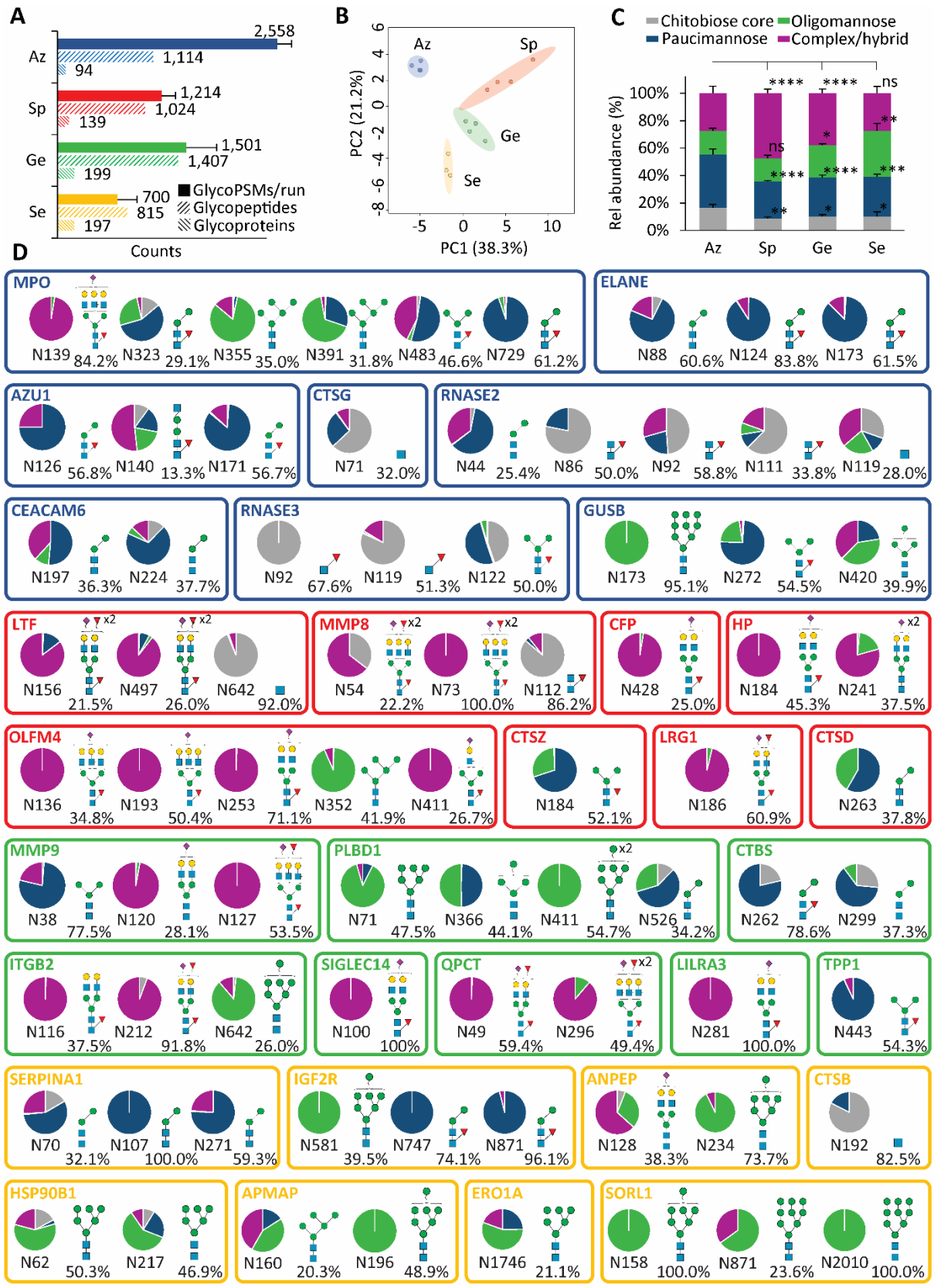

Figure 3. Glycoproteomics reveals site-, protein- and granule-specific *N*-glycosylation across the neutrophil granules. **A)** Glycoproteome coverage across the neutrophil granules

as measured by *N*-glycoPSM counts, unique *N*-glycopeptides (unique protein, site, glycan), and source *N*-glycoproteins identified by quantitative glycoproteomics. GlycoPSM data are plotted as mean ± SD while glycopeptide/glycoprotein data are plotted as total counts from n = 4 biological replicates. **B)** Glycoproteomics-informed PCA of the neutrophil granules (Az, Sp, Ge, Se). **C)** *N*-glycan type distribution across neutrophil granules. Data plotted as mean ± SD (n = 4 biological replicates, $*p < 0.05$, $**p < 0.01$, $****p < 0.0001$, ns, not significant, ANOVA test). **D)** Extensive *N*-glycan diversity across sites and proteins as illustrated for the eight most abundant *N*-glycoproteins (out of 100-200 glycoproteins/granule) across each neutrophil granule. The most abundant glycoform (and its relative site-specific abundance) is indicated for each site. See **Figure 1** for key.

Profound glycoproteome remodelling during neutrophil granulopoiesis

In attempts to unpick the mechanisms driving the intriguing granule-specific *N*-glycosylation in resting neutrophils, we investigated longitudinally the *N*-glycoproteome remodelling accompanying the granulopoiesis process in the bone marrow. Specifically, we mined robust proteomics and transcriptomics data collected from discrete myeloid progenitor stages for previously overlooked *N*-glycopeptide and glyco-enzyme expression patterns[26,27]. Owing to the high data quality, a total of 11,928 *N*-glycoPSMs from 2,276 unique *N*-glycopeptides mapping to 1,079 source *N*-glycoproteins (**Supplementary Figure S2A** and **Supplementary Table S5-S6**) and 45 glyco-enzymes facilitating *N*-glycosylation events (**Supplementary Table S7**) could be longitudinally profiled from these available resources.

In early granulopoiesis (P/M stage), the myeloid progenitors displayed prominent paucimannosylation (~45%) and chitobiose core-type (~25%) *N*-glycosylation, which were dramatically reduced in the subsequent maturation stage (MM stage, ~20% and ~15%, respectively), which instead featured elevated complex- (~15%->35%) and oligomannosidic-

type (~15%->30%) *N*-glycans (**Figure 4A** and **Supplementary Table S5**). The glycoproteome remodelling was notably reduced in mid- (MM) and late- (BN, SN) stage granulopoiesis.

Early myeloid progenitors (P/M stage) indeed showed a distinctly different glycophenotype compared to progenitors in the MM, BN and SN stages as illustrated by the separation of P/M cells by PCA, further supporting that strong *N*-glycoproteome remodelling accompanies early neutrophil maturation (**Figure 4B**). We therefore used transcriptomics to monitor the relative glycoprotein and glyco-enzyme expression during the P/M-to-MM transition (**Figure 4C**). Interestingly, we found that prominent changes in the proteome expression (green) as opposed to the glyco-enzymes (yellow) accompany the *N*-glycoproteome remodelling phase. Expectedly, the Az proteins expressed at the P/M stage (blue, e.g. MPO, AZU1, ELANE) and Sp proteins expressed at the MM stage (red, e.g. HP, LTF, MMP8) showed strong and opposite expression differences (up to 5-30 fold) between the two stages. In fact, ~75% of the transcriptome dataset (2,579/3,484 transcripts) demonstrated expression differences between the P/M and MM stages (Student's t-test, FDR < 0.05, **Supplementary Table S7**).

In line with the prominent protein expression differences and relatively minor changes to the glycosylation machinery during granulopoiesis, the glycosylation of several key proteins enriched in the Az granules but found throughout all granule populations (MPO, AZU1, ELANE, CTSG) remained relatively unchanged during neutrophil maturation (**Figure 4D** and **Supplementary Table S5**). The indistinguishable glycosylation pattern of these proteins when profiled at the SN stage (near-mature cells forming the bone marrow reserve pool of neutrophils) and PMN stage (mature blood neutrophils) indicated, as expected, that only minute differences exist in terms of the glycophenotype between the final stages of bone marrow maturation and fully mature neutrophils in circulation. Taken together, these results therefore indicate that the granule-specific *N*-glycosylation in resting neutrophils is driven primarily by

glycoprotein repertoire changes during granulopoiesis as opposed to prominent global changes in the cellular glycosylation machinery.

As a notable exception, the global expression analysis indicated altered P/M-to-MM expression of the oligosaccharide transferase (OST) enzyme complex responsible for the initiation of *N*-glycoprotein biosynthesis. We therefore used already mentioned -omics resources[26,27] to monitor the transcript- and protein-level expression profile of the subunits forming the OST enzyme complex (STT3A/B, RPN1/2, DDOST, DAD1, OSTC) during granulopoiesis and found considerably reduced OST mRNA (**Figure 4E**) and protein expression (all $p < 0.001$, student's t-test, P/M vs other stages combined) (**Figure 4F**) over the course of neutrophil maturation. Correlating with the observed OST dynamics, proteins expressed at the P/M stage and those identified in the corresponding Az granules displayed greater *N*-glycan occupancy (higher 'glycosylation efficiency') compared to proteins expressed later during differentiation and those residing in other corresponding granules (all $p < 0.05$, student's t-test, P/M/Az vs other maturation stages/granules combined) (**Figure 4G-H**). Collectively, the temporal profiling of the *N*-glycoproteome and the *N*-glycosylation machinery during myeloid differentiation, the first of its kind, have revealed that profound glycoproteome remodelling accompanies granulopoiesis and provides important system-wide molecular-level clues to mechanisms driving the granule-specific *N*-glycosylation observed in circulating neutrophils.

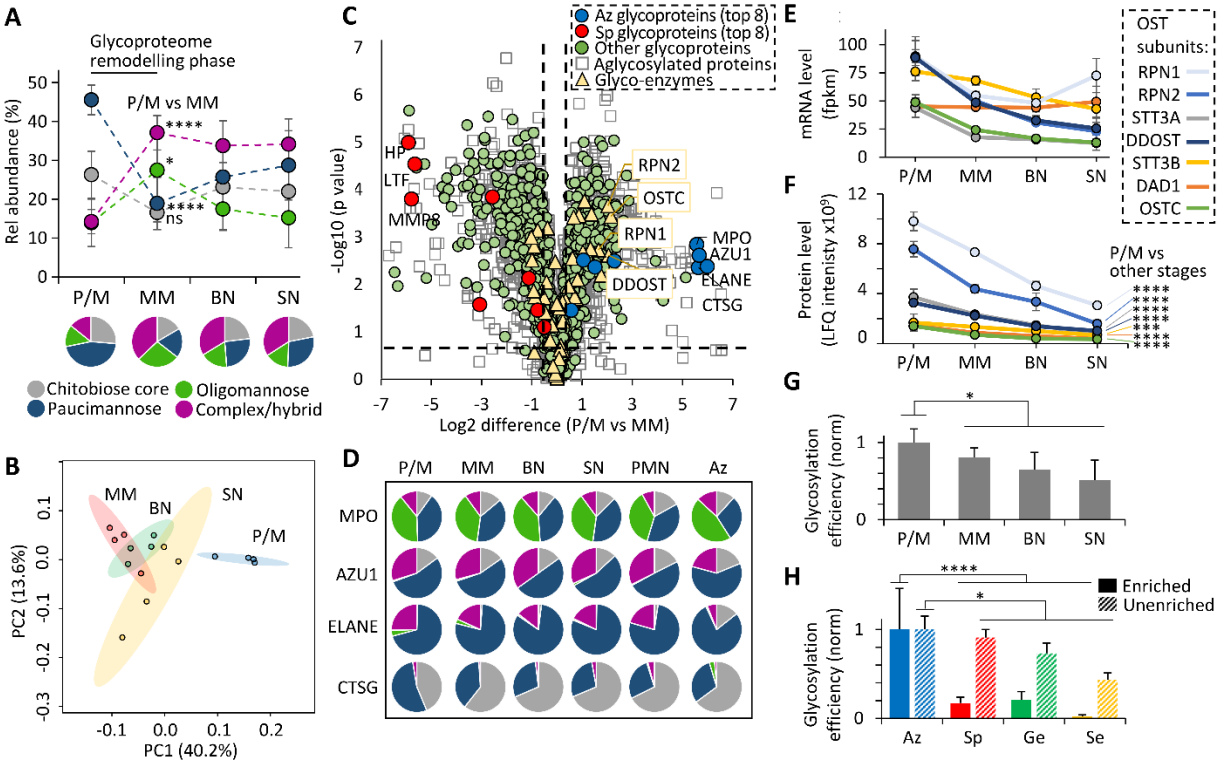

Figure 4. Dramatic glycoproteome remodelling in early granulopoiesis is accompanied by changes in proteome expression and the glycosylation initiation machinery. A) *N*-glycan class distribution during granulopoiesis as established by glycopeptide profiling from proteomics of key myeloid progenitor cell types (P/M, MM, BN, SN)[27]. **B)** *N*-glycopeptide-informed PCA of the four populations of myeloid progenitors. **C)** Differential transcript expression between P/M and MM progenitors. Permutation-based FDRs < 0.05 and S0 > 0.1 were calculated using Perseus. Dashed x/y lines represent significance thresholds. Proteins were assigned with granule location/glycosylation status based on glycoproteomics data (**Supplementary Tables S4**). Key *N*-glycosylation enzymes (yellow) including OST subunits (boxed, yellow) and the eight most abundant Az (blue) and Sp (red) glycoproteins amongst other glycosylated (green) and non-glycosylated (white) proteins are highlighted. **D)** Uniform *N*-glycosylation of key Az glycoproteins during granulopoiesis, in blood neutrophils (PMN) and in their principal granule location ('Az') of resting neutrophils. For simplicity, multiple sites were combined for the glycoprofile of MPO, AU1 and ELANE. **E)** Transcript (mRNA)

and **F)** protein expression profile of the OST subunits during myeloid differentiation. Data plotted as mean ± SD (n = 4 biological replicates, ***$p < 0.001$, ****$p < 0.0001$, student's t-tests, P/M vs other stages combined). Global protein *N*-glycosylation efficiency **G)** during granulopoiesis and **H)** across the corresponding neutrophil granules mapped separately for enriched (full bars) and unenriched (broken bars) glycoproteomics data. Data plotted as mean ± SD (n = 4 biological replicates. *$p < 0.05$, ****$p < 0.0001$, student's t-tests, P/M vs other stages combined. See **Figure 1** for key.

Discussion

Neutrophils store cytosolic granules packed with highly glycosylated and potent hydrolytic enzymes, membrane receptors and microbicidal glycoproteins that can be mobilised in a timely and coordinated manner to allow neutrophils to traffic to sites of infection and fight invading pathogens[30]. While literature have documented diverse roles for protein *N*-glycosylation in neutrophil function[4], the structural diversity and spatial distribution of the *N*-glycoproteome across the neutrophil granules and the temporal dynamics during the profound metamorphosis underpinning neutrophil granulopoiesis remain unmapped. Closing this knowledge gap is important since while under normal physiology and homeostasis neutrophils play protective roles throughout the body, it is becoming increasingly apparent that neutrophils can also, under certain conditions, play disease-promoting roles upon dysregulation of processes directly or indirectly involving protein glycosylation including impaired neutrophil maturation, recruitment, activation and turnover[4,31,32].

In this study, we therefore employed an integrated glycomics-assisted glycoproteomics method[25] to comprehensively profile the *N*-glycoproteome of granule populations from resting neutrophils. The initial *N*-glycome profiling facilitated a quantitative view of the glycan fine structures and aided the informative (yet challenging[29]) *N*-glycoproteomics data analysis

enabling us to establish with high precision the, to date, most detailed quantitative map of the heterogeneous *N*-glycoproteome across four major granule populations of human neutrophils (Az, Sp, Ge, Se). Further, deep mining of *N*-glycopeptide and glyco-enzyme expression patterns using robust proteomics[27] and transcriptomics[26] resources obtained from discrete myeloid progenitor types unveiled, with temporal resolution, the dynamic proteome expression and non-template-driven glycosylation processes accompanying neutrophil granulopoiesis.

Expanding significantly on previous efforts aiming to globally map neutrophil *N*-glycosylation events[12-14], we here provide direct evidence for the distinctive glycophenotypes exhibited by the four investigated neutrophil granule populations and report on site-specific *N*-glycan features and carrier protein repertoires contributing to the intriguing granule-specific *N*-glycosylation observed in blood neutrophils.

The Az granules, which consistently displayed the most distinctive *N*-glycosylation signatures, exhibited elevated levels of unconventional paucimannosidic-, chitobiose core- and monoantennary complex-type *N*-glycans. Recapitulating observations from targeted protein structure-function studies[12,15,17,18], these unusual *N*-glycosylation features were found to be carried by MPO, ELANE and CTSG amongst ~100 other less studied Az glycoproteins. The discovery of peculiar *N*-glycosylation in the Az granules is interesting as this compartment is regarded as the microbicidal granule that neutrophils mobilise both intra- and extracellularly when combating pathogens at infection sites[3,30]. While the observation that unconventional *N*-glycans decorate a diverse repertoire of potent Az proteins is intriguing, their role(s) in shaping the microbicidal potential of the Az granules remains largely unstudied[4,21]. Our report of a bacteriostatic potential of the paucimannosidic *N*-glycans carried by ELANE towards clinical strains of *Pseudomonas aeruginosa* is, to our knowledge, the only literature on this topic[15].

In addition to phagosomal fusion, a subset of the Az granules degranulate their content into the extracellular environment upon neutrophil activation[33]. Thus, there is also the potential for the

unconventional glycosylation of the Az proteins to mediate cell-cell communication through putative signalling receptors towards paucimannose[20] and induce production of autoantibodies in neutrophil-related auto-immune diseases, such as anti-neutrophil cytoplasmic autoantibody-associated vasculitis as speculated by others[18]. Supporting the former, we and others have demonstrated that mannan-binding lectin (MBL2, P11226)[12] and the macrophage mannose receptor (CD206, P22897)[34] display affinities to paucimannosidic glycoepitopes, but lectin receptors with high affinity/avidity to paucimannose and any cell-cell communication and other functional consequences resulting from their interaction require further exploration. Since neutrophil-derived MPO reportedly is internalised via endocytosis by CD206 on macrophage cell surfaces[35], paucimannosylation may proposedly also function as danger associated molecular patterns[36] or alternatively serve as 'removal tags' of the potent (thus potentially harmful) Az proteins to prevent damage to host tissues following excessive release and pathogen killing, speculations also demanding empirical support.

Our finding that biologically-relevant Lewis (Le) and sialyl-Lewis (sLe) glycoepitopes decorate a considerable subset of the ~140 glycoproteins e.g. LTF, MMP8 (P22894), LRG1 (P02750) identified in the Sp granules is in line with (but considerably expands on) existing literature[14,37,38]. The Lewis-type epitopes are known to mediate neutrophil tethering and rolling, and, in turn, facilitate extravasation to inflammatory sites through interactions with endothelial selectins[39]. However, literature points primarily to membrane-embedded glycoproteins residing in readily mobile secretory vesicles e.g. PSGL-1 (Q14242), ESL-1 (Q92896), CD44 (P16070) being responsible for this process[4]. Interestingly, our study reveals that many luminal (soluble) Sp glycoproteins also carry s/Le glycoepitopes. The extracellular roles of these glycoproteins remain essentially unstudied apart from a few reports suggesting that Le^x on luminal Sp glycoproteins (e.g. LTF) mediates binding to the scavenger receptor C-type lectin (SRCL, Q5KU26) expressed on endothelial cells throughout the vasculature to facilitate

internalisation and clearance of these bioactive (and potentially harmful) glycoproteins[37,40]. Despite enabling detailed *N*-glycome mapping, a limitation of our PGC-LC-MS/MS glycomics approach is that the exact glycoepitopes (s/Le$^{a/x}$, s/Le$^{b/y}$) in many cases could not be unambiguously defined due to the complexity/size of such *N*-glycans. In previous efforts, we used glycan-directed antibodies to indicate that Le^{x} and sLe^{x} dominate the Sp/Ge and Se compartments, respectively[14], but these fine structural aspects still require detailed elucidation. Finally, the Ge and Se granules each hosted ~200 *N*-glycoproteins carrying predominantly oligomannosidic- and less sialylated/fucosylated complex-type *N*-glycans. While traditionally regarded as an intracellular glyco-feature pertaining to immaturely-processed *N*-glycoproteins trafficking the secretory machinery, oligomannosylation is increasingly reported i) on mature (fully processed) neutrophil glycoproteins as comprehensively reviewed[4,20], ii) to decorate the surface of neutrophils[41] and other blood[42] and epithelial[43,44] cells, and iii) to be elevated in cancer[45,46] and other neutrophil-related diseases[47]. Our study supports that oligomannosylation is a prominent feature of the Ge and Se compartments. This is of potential significance since neutrophils readily expose, in a context-dependent manner, their granule content from the mobile granules/vesicles to the extracellular environment to enable cell-cell communication with surrounding tissues or removal from circulation as previously discussed[4,20].

Opposing a recent study suggesting (via inference) that M6P-oligomannosylation is a prominent glyco-feature of the Az granules[13,48], our complementary and quantitative glycomics and glycoproteomics data demonstrated low abundance of M6P-oligomannosylation across all neutrophil granules (0.5-1% of *N*-glycome) indicating that this modification may previously have been over-estimated, possibly due to experimental conditions favouring M6P-detection. In support, we previously found poor M6P-modification levels upon targeted MPO profiling using orthogonal analytical workflows[17]. Moreover, relatively few diagnostic fragment ions specific for M6P-glycans (*m/z* 241) and glycopeptides (*m/z* 243) were detected in the wealth

of LC-MS/MS data generated by this study (data not shown). We are, however, unable to document if our sample handling procedures quantitatively preserved all M6P-modifications. Intriguingly, the neutrophil granule *N*-glycoproteome was devoid of bisecting GlcNAc and comprised only trace levels of hybrid-type *N*-glycans, two relatively common structural features of most human cell/tissue types. Since neutrophils clearly produce the relevant biosynthetic *N*-glycan substrates and express both MGAT1 and MGAT3 (as evaluated by transcriptomics, data not shown) required for the formation of hybrid-type *N*-glycans and bisecting GlcNAcylation, respectively, their (near) absence may suggest other biosynthetic mechanisms at play including the putative involvement of lysosomal α-mannosidases (e.g. MAN2B1, O00754) and *N*-acetylhexosaminidase isoenzymes (Hex, P06865/P07686) known to be highly expressed in Az granules of neutrophils. In fact, excessive α-mannosidase activity on hybrid-type intermediates serves as a convenient explanation for the abundance of peculiar monoantennary complex-type *N*-glycans in the Az granules. Related to this, we recently demonstrated that Hex drives paucimannose formation in a non-canonical truncation pathway and suggested in the same study truncation-mediating roles of lysosomal α-mannosidases in human neutrophils[19]. The substrate-specificity of Hex and lysosomal α-mannosidase for bisecting GlcNAc and hybrid-type *N*-glycans, however, requires documentation. Relevant also to this hypothesis, we previously noted a peculiar absence of *O*-glycosylation in the Az granules whereas extended LacNAc-rich core-2 *O*-glycans were found in the Sp, Ge and Se granules[14]. Since our mining of transcriptomics data suggests that several Golgi-based GalNAcTs responsible for *O*-glycan initiation are constitutively expressed during granulopoiesis (data not shown), the absence of *O*-glycosylation in Az granules may indicate that co-trafficking with Hex during the P/M maturation stages quickly removes *O*-GalNAc residues once added preventing further elongation of *O*-glycosylation in these compartments. In addition to protein *N*- and *O*-glycosylation, neutrophils also express glycosaminoglycans,

proteoglycans and glycosphingolipids, all of which are known to play roles in neutrophil function[49-51]. Future research is required to explore the granule distribution and potential granule-specific functions of these glycoconjugates.

Excitingly, our investigation of myeloid progenitors in different maturation stages revealed considerable plasticity in key *N*-glycosylation processes and detailed a global remodelling of the *N*-glycoproteome during neutrophil granulopoiesis. Particularly dramatic *N*-glycoproteome remodelling was found to accompany early maturation (P/M-to-MM transition). Notably, the Az and Sp granules formed during the P/M and MM differentiation stages, respectively, exhibited striking glycoproteome differences providing important mechanistic clues to the formation of the distinct glycoproteome characteristics across the granule populations. The P/M-to-MM transition is important as it marks the change from self-replicating promyelocytes to non-dividing and committed metamyelocytes, a transition that is accompanied with notable phenotypic (morphological, molecular, functional) alterations[27]. This is, to the best of our knowledge, the first report to demonstrate glycoproteome remodelling in developing myeloid progenitor cells. In fact, maturation stage-specific glycosylation appears scarcely investigated with recently available and highly informative glycoproteomics approaches. Examples from the glycobiological literature include our own report on dynamic glycosylation underpinning myogenesis and muscle development[52], and *N*-glycoproteome changes during neuronal[53], and cardiomyocyte[54] differentiation reported by other groups.

Importantly, our multi-omics interrogations established that the *N*-glycoproteome remodelling occurring during granulopoiesis is driven primarily by temporal changes in the proteome expression patterns leading to different glycoprotein repertoires across the individual granule populations. Less prominent were changes within the glycosylation machinery responsible for the enzymatic processing of nascent *N*-glycoproteins trafficking the secretory pathway. Supporting a strong proteome- (as opposed to glyco-enzyme-) based regulation, we observed

surprisingly poor correlations between many of the observed granule-specific *N*-glycan features (e.g. core/antenna fucosylation, α2,3-/α2,6-sialylation, Figure 2C) and expression levels of corresponding biosynthetic enzymes (e.g. fucosylTs, sialylTs, data not shown). This observation is important as it illustrates alternative factors (other than the glycosylation machinery) mediating glycoproteome remodelling in neutrophils, and serves to explain how some *N*-glycoproteins expressed throughout granulopoiesis (e.g. MPO, ELANE) can receive relatively uniform glycosylation regardless of the timing of their expression and their granule location (Figure 4D). To this end, both the protein repertoire and the glycosylation machinery can be considered determinants for the distinct glycophenotypes of the neutrophil granules. However, beyond relatively simple solvent accessibility><glycan processing relationships[55], a molecular level understanding of how neutrophil proteins carry information that enable their individualised modification patterns across the neutrophil granules (e.g. high α2,6-sialylation and low antennary fucosylation for Az proteins) is still lacking. Finally, we acknowledge that other dynamic factors such as Golgi restructuring, altered micro-trafficking routes and changes to the non-enzymatic components of the glycosylation machinery (i.e. nucleotide-sugar transporters and substrate levels), all of which were not explored in this study, may also accompany granulopoiesis, which consequently add another level of complexity to consider in our attempt to decode mechanisms governing the complexity of the neutrophil glycoproteome. As a notable exception to the relatively stable glycosylation machinery during neutrophil granulopoiesis, expression of the OST enzyme complex responsible for the initiation of *N*-glycoprotein biosynthesis was significantly reduced during neutrophil maturation, which correlated with a relatively high glycosylation efficiency in the Az granules relative to other granules (Figure 4E-H). We are not aware of similar reports of OST dynamics during the maturation of neutrophils (or other cell types), but a growing body of evidence points to context-dependent OST regulation and interesting links to cancer, immune evasion and ER

stress[56,57]. It is tempting to speculate that Az proteins require high glycosylation occupancy to prevent premature proteolytic degradation during the extended storage in these highly hydrolytic compartments hosting many potent proteases (e.g. ELANE, CTSG). Although energetically expensive, the installation of voluminous and flexible glycans on protein surfaces is in fact shown confer effective protection against proteolysis[58,59].

In steady-state conditions, neutrophils form from haematopoietic stem and progenitor cells in the bone marrow[1]. However, during systemic infection and inflammation involving a prolonged demand for neutrophils (e.g. cancer and chronic infections), the haematopoietic system switches from steady-state to 'emergency granulopoiesis'[60,61]. This so-called 'left-shift' results in the appearance of neutrophil precursors in circulation featuring immature phenotypes including aberrant (progenitor-like) morphology and, presumably, an incomplete repertoire of granules and/or granule content. Considering our discovery of maturation stage-specific glycosylation, we hypothesise that immature neutrophils arising from emergency granulopoiesis display an "immature" (not fully remodelled) *N*-glycoproteome[4]. Impaired granulopoiesis is also central to acute myeloid leukemia (AML)[62], in which morphologically immature blood neutrophils, expectedly exhibiting aberrant glycosylation, were found to show decreased capacity for NET formation[63]. The link (if any) between poor NET formation and aberrant glycosylation of AML neutrophils remains to the best of our knowledge unexplored. Guided by our *N*-glycoproteome map of healthy neutrophils communicated herein, future glycoprofiling efforts of immature neutrophils from individuals exhibiting emergency granulopoiesis and AML patients are required to substantiate these speculations and establish causal links to neutrophil dysfunction.

In conclusion, our detailed spatiotemporal *N*-glycoproteome profiling of developing myeloid progenitors and mature neutrophils has painted the, to date, most comprehensive picture of the intriguingly complex neutrophil *N*-glycoproteome and has laid an important foundation to

explain its formation. Our systems glycobiology (multi-omics) approach revealed that strong *N*-glycoproteome remodelling underpins neutrophil granulopoiesis, which, when considered with the widely accepted 'targeting by timing' model[6,7], provides new mechanistic clues to the distinctive glycophenotypes exhibited by each neutrophil granule population as detailed herein. Importantly, our data-rich omics-centric study serves as a valuable resource to guide future explorations targeting the biological roles and dysregulation of neutrophil glycosylation that holds an untapped clinical potential for the discovery of glycoprotein-related markers for and therapeutics against a spectrum of neutrophil-related disorders.

Acknowledgments

RK is supported by the Cancer Institute of New South Wales (ECF181259). JU is supported by a Macquarie Research Excellence Scholarship. SC was supported by an International Macquarie Research Excellence Scholarship (iMQRES 2017152). IL was supported by an International Research Training Program Scholarship funded by the Australian Government. HCT was supported by a Macquarie University COVID-19 fellowship. ZSB was supported by a JSPS fellowship. JB was supported by grants from the Swedish Research Council (2019-01123) and TUA Research Funding; The Sahlgrenska Academy at University of Gothenburg/Region Västra Götaland, Sweden (TUAGBG-917531). AKB is supported by the Swedish Research Council (2018-03077). MTA is supported by an Australian Research Council Future Fellowship (FT210100455).

Author contributions

RK, JU, IL and MTA designed experiments. RK, SC, HT, IL, BLP and VV conducted experiments. RK, RD, ZSB, AKB, JB and MTA established laboratory methodologies. RK, JU, SC, HT, IL, MTA analysed the data. BLP, VV, RD, AKB and JB provided reagents for

this study. RK, JU and MTA wrote the manuscript. RK and MTA supervised this study and acquired funding. All authors have reviewed and approved the manuscript.

Declaration of interests

The authors declare no competing interests.

Main figure titles and legends

Figure 1. Spatiotemporal *N*-glycoproteome profiling of neutrophil granules and myeloid maturation stages using systems glycobiology approaches. A) Spatial *N*-glycoproteome profiling using quantitative glycomics-assisted glycoproteomics of the four major granule populations isolated from resting neutrophils. **B)** Temporal profiling of the *N*-glycoproteome and the underpinning glycosylation machinery of discrete neutrophil maturation stages from bone marrow-derived myeloid progenitor cells through interrogation of available proteomics and transcriptomics resources[26,27]. Neutrophil granule isolation was orthogonally validated using the generated proteomics data by **C)** plotting the expression profile of known neutrophil granule markers i.e. myeloperoxidase (MPO) for azurophilic granules (Az), lactoferrin (LTF) for specific granules (Sp), matrix metalloproteinase-9 (MMP9) for gelatinase granules (Ge) and ficolin-1 (FCN1) for the secretory vesicles/plasma membrane (Se) and **D)** concordance of the 50 most abundant proteins identified in the Az granules against a key reference study also performing quantitative proteomics of separated neutrophil granules[7]. See **Supplementary Table S1** for the correlation of other granule datasets. See insert for key to the glycan symbols, linkage nomenclature and the neutrophil granules and maturation stages.

Figure 2. Granule-specific *N*-glycome signatures in resting neutrophils. A) PCA of quantitative *N*-glycomics data of the four granule populations (Az, Sp, Ge, Se) isolated from resting neutrophils. **B)** *N*-glycan class distribution across granules. Key glyco-features across granules including **C)** core/antenna fucosylation and α2,3-/α2,6-sialylation, **D)** mannose-6-phosphate (M6P) modifications and **E)** antennary branching patterns (relative abundance of each glyco-feature against the total *N*-glycome). For panel B-E, data plotted as mean and SD (n = 4 biological replicates, SD left out in panel B for simplicity, ANOVA test, $^{**}p < 0.01$,

****$p < 0.0001$, ns, not significant). **F)** Left: Unsupervised clustering (see **Supplementary Figure S1C** for dendrogram) and heatmap of *N*-glycomics data illustrating four major clusters representing the neutrophil granule populations. Right: *N*-glycan structures contributing to each cluster. The most common structure is depicted for glycan compositions exhibiting multiple isomers. *chitobiose core-type *N*-glycans reported at the glycopeptide level. See Figure 1 for key. See **Supplementary Table S2** for glycan identifiers consistently used throughout the study.

Figure 3. Glycoproteomics reveals site-, protein- and granule-specific *N*-glycosylation across the neutrophil granules. **A)** Glycoproteome coverage across the neutrophil granules as measured by *N*-glycoPSM counts, unique *N*-glycopeptides (unique protein, site, glycan), and source *N*-glycoproteins identified by quantitative glycoproteomics. GlycoPSM data are plotted as mean ± SD while glycopeptide/glycoprotein data are plotted as total counts from n = 4 biological replicates. **B)** Glycoproteomics-informed PCA of the neutrophil granules (Az, Sp, Ge, Se). **C)** *N*-glycan type distribution across neutrophil granules. Data plotted as mean ± SD (n = 4 biological replicates, *$p < 0.05$, **$p < 0.01$, ****$p < 0.0001$, ns, not significant, ANOVA test). **D)** Extensive *N*-glycan diversity across sites and proteins as illustrated for the eight most abundant *N*-glycoproteins (out of 100-200 glycoproteins/granule) across each neutrophil granule. The most abundant glycoform (and its relative site-specific abundance) is indicated for each site. See **Figure 1** for key.

Figure 4. Dramatic glycoproteome remodelling in early granulopoiesis is accompanied by changes in proteome expression and the glycosylation initiation machinery. A) *N*-glycan class distribution during granulopoiesis as established by glycopeptide profiling from proteomics of key myeloid progenitor cell types (P/M, MM, BN, SN)[27]. **B)** *N*-glycopeptide-

informed PCA of the four populations of myeloid progenitors. **C)** Differential transcript expression between P/M and MM progenitors. Permutation-based FDRs < 0.05 and S0 > 0.1 were calculated using Perseus. Dashed x/y lines represent significance thresholds. Proteins were assigned with granule location/glycosylation status based on glycoproteomics data (**Supplementary Tables S4**). Key *N*-glycosylation enzymes (yellow) including OST subunits (boxed, yellow) and the eight most abundant Az (blue) and Sp (red) glycoproteins amongst other glycosylated (green) and non-glycosylated (white) proteins are highlighted. **D)** Uniform *N*-glycosylation of key Az glycoproteins during granulopoiesis, in blood neutrophils (PMN) and in their principal granule location ('Az') of resting neutrophils. For simplicity, multiple sites were combined for the glycoprofile of MPO, AU1 and ELANE. **E)** Transcript (mRNA) and **F)** protein expression profile of the OST subunits during myeloid differentiation. Data plotted as mean ± SD (n = 4 biological replicates, ***$p < 0.001$, ****$p < 0.0001$, student's t-tests, P/M vs other stages combined). Global protein *N*-glycosylation efficiency **G)** during granulopoiesis and **H)** across the corresponding neutrophil granules mapped separately for enriched (full bars) and unenriched (broken bars) glycoproteomics data. Data plotted as mean ± SD (n = 4 biological replicates. *$p < 0.05$, ****$p < 0.0001$, student's t-tests, P/M vs other stages combined. See **Figure 1** for key.

STAR Methods

RESOURCE AVAILABILITY

Lead contact

Further information and requests for resources and reagents should be directed to and will be fulfilled by the lead contact, Morten Thaysen-Andersen (morten.andersen@mq.edu.au).

Materials availability

This study did not generate or make use of new unique reagents.

Data and code availability

To provide an accessible resource featuring comprehensive spatiotemporal information of the neutrophil *N*-glycoproteome for community interrogation and hypothesis generation/testing, all generated LC-MS/MS datasets, search output and metadata have been deposited in public repositories (see below).

Specifically, proteomics search files (.msf) and search results (.pdResult) have been deposited to the ProteomeXchange Consortium via the PRIDE repository and are publicly available as of the date of publication. Accession numbers are listed in the Key Resources Table. Glyco/proteomics LC-MS/MS raw data have been deposited to the ProteomeXchange Consortium via the PRIDE repository. Glycomics LC-MS/MS raw data have been deposited to the GlycoPOST repository. Accession numbers are listed in the Key Resources Table.

This paper analyses existing publicly available data. The accession numbers for these datasets are listed in the Key Resources Table.

This paper does not report or make use of original code.

Any additional information required to reanalyse the data reported in this paper is available from the lead contact upon request.

EXPERIMENTAL MODEL AND SUBJECT DETAILS

Human neutrophils were isolated from buffy coats from individuals without any apparent health issues. Buffy coats were obtained from The Blood Center, Sahlgrenska University Hospital, Gothenburg, Sweden. According to Swedish law on ethical conduct in human research, ethics approval was not needed because the buffy coats were provided anonymously and could not be traced back to a specific individual. For this reason, information of age and gender is not available.

METHOD DETAILS

Neutrophil isolation

Buffy coats (~60 ml) from sixteen healthy individuals without any apparent health issues were obtained from The Blood Center, Sahlgrenska University Hospital, Gothenburg, Sweden. From these samples, four biological replicates (named donor v-z for sample/data labelling purposes) each comprising of a pool of buffy coats from four individuals were investigated. Resting neutrophils were isolated from the pooled buffy coats by removing firstly erythrocytes by dextran (1%) sedimentation (1 x g) and secondly monocytes and lymphocytes by centrifugation on a Ficoll–Paque density gradient. Any remaining erythrocytes were eliminated by hypotonic lysis in a Krebs–Ringer phosphate buffer containing 10 mM glucose and 1.5 mM Mg^{2+} yielding a population of resting neutrophils with >95% purity as assessed by flow cytometry.

Neutrophil granule isolation

Neutrophil granules were separated using an established three-layered Percoll method[28]. Briefly, ~10^9 neutrophils/sample were treated with 8 mM diisopropylfluorophosphate (final concentration), resuspended in 10 ml homogenisation buffer containing 100 mM KCl, 3 mM NaCl, 3.5 mM $MgCl_2$, 10 mM PIPES (pH 7.4) with 1 mM $ATP(Na)_2$, 0.5 mM

phenylmethylsulfonyl fluoride and gently disrupted in a nitrogen bomb (Parr Instruments, Moline, IL, USA) at 400 psi. A density gradient generated by 1.12 g/mL, 1.09 g/mL, and 1.05 g/mL Percoll (GE17-0891-01, GE Healthcare, Sweden) was used to separate the azurophilic (Az) granules, specific (Sp) granules, and gelatinase (Ge) granules and a combined fraction containing the secretory vesicles and the plasma membrane (Se) after centrifugation at 37,000 x g, 4°C, 30 min. The separation of these four neutrophil granules (designed a-d for sample/data labelling purposes) was guided by monitoring known granule markers using established immunoblot and enzyme activity assays across the density fractions as previously demonstrated[14] and orthogonally validated using the acquired proteomics data to map proteins known to be enriched in each compartment.

The pelleted granules were resuspended in the homogenisation buffer (above) and lysed using a tip sonicator at 1/3 power (8 MHz) three times for 30 s on ice. The luminal (soluble) proteins were separated from the membrane (insoluble) proteins of each granule fraction by ultracentrifugation at 100,000 x g, 4°C, 90 min. The supernatants containing luminal proteins were carefully collected and the protein concentrations determined using Bradford assays. The protein samples were stored at a concentration of 4–15 µg/µl at –20°C until further handling.

Glycome profiling

N-glycan release and clean-up

The luminal protein extracts from the neutrophil granules were reduced using 10 mM aqueous dithiothreitol (DTT) in 100 mM NH_4HCO_3 (pH 8.4), 45 min, 56°C, and then carbamidomethylated using 25 mM aqueous iodoacetamide (IAA) in 100 mM NH_4HCO_3 (pH 8.4), 30 min, 20°C, in the dark. The alkylation reactions were quenched using 25 mM aqueous DTT (all final concentrations). The *N*-glycans were released from the protein extracts and prepared for glycomics as described[64]. For each granule sample, ~20 µg total protein was

blotted on a primed 0.45 mm polyvinylidene difluoride membrane (Merck-Millipore), stained with Direct Blue, excised and transferred to separate wells in a flat bottom polypropylene 96-well plate (Corning Life Sciences). Spots were blocked with 1% (w/v) polyvinylpyrrolidone in 50% (v/v) aqueous methanol and washed with water. *N*-glycans were enzymatically released using 3.5 U *Flavobacterium meningosepticum N*-glycosidase F recombinantly expressed in *E. coli* (Roche) in 20 ml H_2O, 16 h at 37°C. The released *N*-glycans were hydroxylated using 100 mM aqueous NH_4HCO_3, pH 5, 1 h, 20°C, and reduced using 1 M $NaBH_4$ in 50 mM aqueous KOH, 3 h, 50°C. The reduction reaction was quenched using glacial acetic acid. Dual desalting of the reduced *N*-glycans was performed using first strong cation exchange resin (where the *N*-glycans are not retained) and then porous graphitised carbon (PGC) (where *N*-glycans are retained) packed as micro-columns on top of C_{18} discs in P10 solid-phase extraction (SPE) formats. The *N*-glycans were eluted from the PGC SPE micro-columns using 0.05% trifluoroacetic acid (TFA) in 40% acetonitrile (ACN) and 59.95% H_2O (v/v/v), dried and reconstituted in 20 µl H_2O, centrifuged at 14,000 x g, 10 min, 4°C and transferred into high recovery glass vials (Waters) for LC-MS/MS analysis. Bovine fetuin was included as a reference glycoprotein to ensure efficient *N*-glycan release and clean-up and to benchmark the LC-MS/MS instrument performance.

N-glycan profile by PGC-LC-MS/MS

Detached *N*-glycan mixtures from each granule sample were injected on a heated (50°C) PGC-LC capillary column (Hypercarb KAPPA, particle/pore size 5 µm/200 Å, column length 100 mm, inner diameter 180 µm, Thermo Fisher Scientific, Australia). Separation of *N*-glycans was carried out over a linear gradient of 0–45% (v/v) ACN (solvent B) in 10 mM aqueous NH_4HCO_3 (solvent A) for 75 min at a constant flow rate of 4 µl/min delivered by a Dionex Ultimate-3000 HPLC system (Sydney, Australia). *N*-glycans were analysed in negative

polarity mode using electrospray ionisation (ESI) on a Velos Pro linear ion trap mass spectrometer (Thermo Fisher Scientific) with a MS1 full scan acquisition range of *m/z* 380-2,000. ESI was performed using an electrospray voltage of 3.2 kV, a nitrogen drying gas flow of 7 l/min at 275°C, and a nitrogen-based nebuliser pressure of 12 psi. An isolation window of 2 *m/z*, a minimum signal of 300 counts and a maximum accumulation time of 30 ms were applied. Data-dependent acquisition was used to select the top nine most abundant precursors in each MS1 full scan spectrum for fragmentation using resonance activation collision-induced dissociation tandem mass spectrometry (CID–MS/MS) at a normalised collision energy (NCE) of 35%. All MS and MS/MS data were acquired in profile mode and dynamic exclusion was disabled. The mass spectrometer was tuned and calibrated using a tune mix (Thermo Fisher Scientific) prior to use.

N-glycan data analysis

Raw data were browsed and interrogated using Xcalibur v2.2 (Thermo Fisher Scientific). GlycoMod (http://www.expasy.ch/tools/glycomod) and GlycoWorkBench v2.1[65] (https://code.google.com/archive/p/glycoworkbench/) assisted the otherwise manual *de novo* glycan annotation as described[66]. Briefly, *N*-glycans were identified based on monoisotopic precursor mass, MS/MS fragmentation pattern and relative and absolute PGC-LC retention time. EIC-based glycan quantification was performed using Skyline v.19.1[67,68]. GlycoWorkBench v2.1[65] (https://code.google.com/archive/p/glycoworkbench/) was used to aid the manual annotation of glycan fragment spectra and to generate glycan cartoons. Glycomics raw data are available from GlycoPost (accession number GPST000315).

Glycoproteome profiling

Protein digestion

The protein extracts from the luminal fraction of the neutrophil granule preparations were precipitated overnight using acetone at -20°C. The pelleted proteins were resuspended in 100 mM aqueous ammonium bicarbonate to a final protein concentration of 0.1 µg/ml. Proteins were then reduced using 10 mM aqueous DTT, 56°C, 45 min, and alkylated using 25 mM aqueous IAA, 25°C, 30 min in the dark (all final concentrations). The alkylation reactions were quenched using 30 mM aqueous DTT in 100 mM aqueous NH_4HCO_3, 25°C, 30 min. The proteins were then exhaustively digested using sequencing-grade modified porcine trypsin (Promega, Australia) at a 1:30 enzyme:substrate ratio (w/w) in 100 mM aqueous NH_4HCO_3, pH 8.4, 37°C, 16 h. Digestions were stopped by acidification with 1% (v/v) aqueous formic acid (FA, final concentration). The resulting peptide mixtures were desalted using C18-SPE micro-columns (Merck-Millipore, Australia). The desalted peptide mixtures were dried and redissolved in 10 µl 0.1% (v/v) aqueous FA for LC-MS/MS.

Glycopeptide enrichment

Glycopeptide enrichment was performed as described[15]. In short, dried peptides were dissolved in 10 µl loading solvent consisting of 80% ACN:1% TFA:19% H_2O (v/v/v), and then applied to custom-made hydrophilic interaction liquid chromatography (HILIC) SPE micro-columns packed to a column height of 22 mm in GELoader tips (Eppendorf, Australia) with zwitterionic HILIC resin (ZIC-HILIC, 10 µm particle size, 200 Å pore size, kindly donated by Merck KGaA, Darmstadt, Germany) on top of C8 Empore SPE discs (Sigma-Aldrich). The micro-columns were equilibrated in 50 µl loading solvent. Approximately 70% of each peptide sample was loaded and reloaded in successive rounds before the micro-columns were washed twice with 50 µl loading solvent. The retained glycopeptides were eluted twice with 50 µl 1% (v/v) aqueous TFA and then with 50 µl loading solvent to ensure complete glycopeptide elution. The eluted fractions were combined and used for LC-MS/MS analysis (enriched glycopeptide

fractions). The remaining 30% of each peptide sample was used directly for LC-MS/MS analysis (unenriched peptide fractions) after desalting on C18 SPE micro-columns packed in stage tips (Merck-Millipore).

Peptide and glycopeptide profiling by reversed-phase LC-MS/MS

The unenriched peptide fractions were analysed using a Q-Exactive HF-X Hybrid Quadrupole-Orbitrap mass spectrometer (Thermo Scientific, Australia) coupled to an Easy nLC-1200 HPLC system (Thermo Scientific, Australia). The mass spectrometer was operated in positive ion polarity mode. Peptides were separated using reversed-phase C18 chromatography using a nano-LC column packed in-house with C18AQ resin (1.9 µm particle size, 120 Å pore size, 0.075 mm inner diameter x 500 mm length, Dr Maisch HPLC GmbH, Germany). The mobile phases were 0.2% FA:19.8% H_2O:80% (v/v/v) ACN (solvent B) and 0.1% (v/v) aqueous FA (solvent A). The linear gradient of solvent B increased from 5-30% over 120 min, 30-60% over 5 min, 60-95% over 5 min and was kept for 5 min at 95% B. The flow rate was kept constant at 300 nl/min. The MS1 acquisition range was *m/z* 350-1,650 at a resolution of 60,000 (measured at *m/z* 200). The MS1 automatic gain control (AGC) target was 3 x 10^6 with a maximum injection time of 50 ms. Data-dependent acquisition was used to select the fifteen most abundant precursors in each MS1 scan for MS/MS using higher-energy collisional dissociation (HCD) at 27% NCE. Precursor isolation windows of *m/z* 1.4 were used. The MS/MS AGC target was 1 x 10^5, the maximum injection time was 25 ms and the resolution was 15,000 (measured at *m/z* 200). Already selected precursors were dynamically excluded for 20 s. Unassigned, singly charged precursors and highly charged precursors ($Z > 8$) were excluded for MS/MS.

The enriched glycopeptide fractions were analysed using an Orbitrap Fusion (Thermo Scientific) coupled to a Dionex 3500RS HPLC system. Glycopeptides were separated using

reversed-phase C18 chromatography using a heated (45°C) nano-LC column packed in-house with C18AQ resin (1.9 µm particle size, 120 Å pore size, 0.075 mm inner diameter x 500 mm length, Dr Maisch HPLC GmbH, Germany) with a gradient of 5 –33% solvent B over 115 min at 300 nl/min. MS1 scans were acquired in the range *m/z* 350 –1,800 (120,000 resolution, 4 x 10^5 AGC, 50 ms injection time) followed by HCD-MS/MS data-dependent acquisition of the seven most intense precursor ions featuring the highest charge state. Fragments were detected in the Orbitrap (30,000 resolution, 2 x 10^5 AGC, 120 ms injection time, 40 NCE, 2 *m/z* quadrupole isolation width). Already selected precursors were dynamically excluded for 60 s. The acquisition strategy included a product ion triggered re-isolation of precursor ions if glycopeptide-specific HexNAc oxonium ions (*m/z* 138.0545, 204.0867, 366.1396) were detected amongst the top 20 fragment ions in each HCD-MS/MS spectrum. The re-isolated precursor ions were subjected to both ETD- and CID-MS/MS analysis. ETD-MS/MS fragments were detected in the Orbitrap (30,000 resolution, 2 x 10^5 AGC, 120 ms injection time, 2 *m/z* quadrupole isolation width, calibrated charge-dependent ETD reaction times enabled) and CID-MS/MS fragments were detected in the ion trap (rapid scan rate, 2 x 10^4 AGC, 70 ms injection time, 30% NCE, 2 *m/z* quadrupole isolation width).

Proteomics and glycoproteomics LC-MS/MS data were acquired from four biological replicates from each of the Az, Sp and Ge granule populations and three biological replicates for the Se fraction due to the loss of a biological replicate during sample build-up.

Proteomics data analysis

For protein identification and quantification, the raw files were imported into MaxQuant v1.6.10.43[69]. The Andromeda search engine was used to search the HCD-MS/MS data against the reviewed UniProtKB Human Protein Database (released December 2019; 20,364 entries) with a precursor and product ion mass tolerance of 4.5 ppm and 20 ppm, respectively.

Carbamidomethylation of cysteine (57.021 Da) was set as a fixed modification. Oxidation of methionine (15.994 Da) and protein N-terminal acetylation (42.010 Da) were selected as variable modifications. All identifications were filtered to 1% protein FDR using a conventional decoy approach. For label-free AUC-based quantification, the 'match between runs' feature of MaxQuant was enabled with a 0.7 min match time window and 20 min alignment time window. Protein abundance was calculated based on the normalised protein intensity (LFQ intensity)[70].

Glycopeptide identification and quantification

Glycopeptides were identified and quantified from the HCD-MS/MS data using Byonic v4.5.2 (Protein Metrics Inc) operated as a node in Proteome Discoverer v.2.5. Search parameters included the use of i) a human proteome database (UniProtKB, 20,416 entries, downloaded August 2019), ii) a glycomics-informed *N*-glycan database comprising the 47 *N*-glycan compositions identified with glycomics of the same samples, iii) a search strategy permitting up to one *N*-glycan per peptide as a "rare" variable modification, semi-trypsin cleavage patterns with a maximum of two missed tryptic cleavages per peptide, up to 10/20 ppm mass tolerance of precursor/product ions from expected values, and up to one Met oxidation (+15.994 Da) per peptide (variable "common" modification), and by using monoisotopic correction (error check = +/- floor (mass in Da / 4,000)), and a decoy and a default contaminant database available in Byonic. Glycopeptide identifications were filtered to FDR < 1% (high confidence as determined using Proteome Discoverer 2.5). Glycopeptides identified with lower confidence, and those found in the decoy and contaminant database were excluded. Quantitation of (glyco)peptides was based on the area-under-the-curve of extracted ion chromatograms of precursor ions as determined by the Minora Feature Detector with the minimum trace length set to 5 and maximum delta retention time of isotope pattern multiplets of 0.2 min within

Proteome Discoverer v2.5. The feature mapper tool was enabled to allow chromatographic alignment of signals and extraction of precursor area based on a matched retention time and *m/z* within a time and mass tolerance window determined automatically by the software. Minimum S/N thresholds were enabled. The matching CID- and ETD-MS/MS spectra were used to manually confirm the glycopeptide identity including glycan structure and glycosylation sites of glycopeptides of particular interest but were neither used for quantitation nor comparison across conditions. Relative glycopeptide quantification was performed by dividing the area of each peptide by the summed area of all peptides within each sample. The quantification of the site-specific glycoform distribution was performed by dividing the area of each glycoform by the summed area of all glycoforms identified within the same site from the same glycoprotein. For comparisons of the glycan composition/glycan class distribution across granules and fractions, glycoPSM counts were used and normalised against the total glycoPSM counts from each sample. For glycoproteome quantification during neutrophil maturation, glycoPSM counts were used with a subtraction approach involving subtraction of glycoproteins identified in the maturation stage(s) prior to the specific maturation stage being assessed (hence only considering newly expressed glycoproteins at each stage). The relative glycosylation efficiency (measure of relative glycan occupancy) was established by dividing the summed area of all glycopeptides by the summed area of all non-glycosylated peptides from the same samples. The glycoproteomics and proteomics raw files are available from the ProteomeXchange consortium via PRIDE accession numbers PXD039387 and PXD021131, respectively.

Interrogation of available proteomics and transcriptomics resources

Proteomics data of neutrophil precursors from four discrete maturation stages isolated by fluorescence-activated cell sorting of myeloid progenitor cells derived from the bone marrow

of four healthy donors were obtained from the ProteomeXchange consortium via the PRIDE partner (data accession number PXD013785)[27]. The investigated maturation stages include the promyelocytic and myelocytic stage (collectively referred to as P/M), metamyelocytic stage (MM), immature neutrophils with band-formed nuclei (BN), and mature neutrophils with segmented nuclei (SN). Circulating (mature, resting) neutrophils (polymorphonuclear cells, PMN) derived from blood from the same four donors were also investigated. Multiple LC-MS/MS datasets (technical replicates) were available for each of these cell populations. For our study, a single technical replicate from each maturation stage from each of the four donors was interrogated given the existence of biological replicates.

RNAseq transcriptome data of neutrophils derived from blood and maturing neutrophils (P/M, MM, BN, SN) isolated from bone marrow of three healthy donors was obtained from Grassi et al.[26] and available at https://blueprint.haem.cam.ac.uk/neutrodiff. Proteomics and related RNA-seq data of the OST enzyme complex were obtained from the Supplementary Table S1 from Hoogendijk et al.[27].

Quantitation and statistical analyses

Statistical significance was assessed using unpaired two-tailed Student's t-tests or ANOVA followed by Tukey test for multiple comparison with FDR < 0.05 as the confidence threshold. For transcriptomics and glycomics data analyses, the *p* value was corrected for multiple test comparison and values below 0.05 were considered significant. GraphPad Prism v9.4.1 (Dotmatics) and Perseus v2.0.7.0[71] were used for the statistical analysis. Correlation analysis was carried out using Pearson correlation coefficient using Excel. PCA analysis was performed using Metaboanalyst v. 5.0[72].

Supplementary Tables

Supplementary Table S1. Proteome profiles of neutrophil granules (AUC-based quant).

Supplementary Table S2. *N*-glycome profiles of neutrophil granules (AUC-based quant).

Supplementary Table S3. *N*-glycoproteome profiles of neutrophil granules (glycoPSM quant).

Supplementary Table S4. *N*-glycoproteome profiles of neutrophil granules (AUC-based quant).

Supplementary Table S5. *N*-glycoproteome profiles of myeloid progenitors (glycoPSM quant).

Supplementary Table S6. *N*-glycoproteome profiles of myeloid progenitors (AUC-based quant).

Supplementary Table S7. Gene expression datasets from P/M vs MM progenitors.

Supplementary Data

Supplementary Data S1. Structural evidence for reported *N*-glycans based on PGC-LC-MS/MS *N*-glycomics data.

References

1. Liew, P.X., and Kubes, P. (2019). The Neutrophil's Role During Health and Disease. Physiol Rev *99*, 1223-1248. 10.1152/physrev.00012.2018.
2. Rosales, C. (2018). Neutrophil: A Cell with Many Roles in Inflammation or Several Cell Types? Front Physiol *9*, 113. 10.3389/fphys.2018.00113.
3. Cowland, J.B., and Borregaard, N. (2016). Granulopoiesis and granules of human neutrophils. Immunol Rev *273*, 11-28. 10.1111/imr.12440.
4. Ugonotti, J., Chatterjee, S., and Thaysen-Andersen, M. (2021). Structural and functional diversity of neutrophil glycosylation in innate immunity and related disorders. Mol Aspects Med *79*, 100882. 10.1016/j.mam.2020.100882.
5. Borregaard, N., and Cowland, J.B. (1997). Granules of the human neutrophilic polymorphonuclear leukocyte. Blood *89*, 3503-3521.
6. Le Cabec, V., Cowland, J.B., Calafat, J., and Borregaard, N. (1996). Targeting of proteins to granule subsets is determined by timing and not by sorting: The specific granule protein NGAL is localized to azurophil granules when expressed in HL-60 cells. Proc Natl Acad Sci U S A *93*, 6454-6457. 10.1073/pnas.93.13.6454.
7. Rorvig, S., Ostergaard, O., Heegaard, N.H., and Borregaard, N. (2013). Proteome profiling of human neutrophil granule subsets, secretory vesicles, and cell membrane: correlation with transcriptome profiling of neutrophil precursors. J Leukoc Biol *94*, 711-721. 10.1189/jlb.1212619.
8. Babu, P., North, S.J., Jang-Lee, J., Chalabi, S., Mackerness, K., Stowell, S.R., Cummings, R.D., Rankin, S., Dell, A., and Haslam, S.M. (2009). Structural characterisation of neutrophil glycans by ultra sensitive mass spectrometric glycomics methodology. Glycoconj J *26*, 975-986. 10.1007/s10719-008-9146-4.
9. Foxall, C., Watson, S.R., Dowbenko, D., Fennie, C., Lasky, L.A., Kiso, M., Hasegawa, A., Asa, D., and Brandley, B.K. (1992). The three members of the selectin receptor family recognize a common carbohydrate epitope, the sialyl Lewis(x) oligosaccharide. J Cell Biol *117*, 895-902. 10.1083/jcb.117.4.895.
10. Nimrichter, L., Burdick, M.M., Aoki, K., Laroy, W., Fierro, M.A., Hudson, S.A., Von Seggern, C.E., Cotter, R.J., Bochner, B.S., Tiemeyer, M., et al. (2008). E-selectin receptors on human leukocytes. Blood *112*, 3744-3752. 10.1182/blood-2008-04-149641.
11. Venkatakrishnan, V., Thaysen-Andersen, M., Chen, S.C., Nevalainen, H., and Packer, N.H. (2015). Cystic fibrosis and bacterial colonization define the sputum N-glycosylation phenotype. Glycobiology *25*, 88-100. 10.1093/glycob/cwu092.
12. Thaysen-Andersen, M., Venkatakrishnan, V., Loke, I., Laurini, C., Diestel, S., Parker, B.L., and Packer, N.H. (2015). Human neutrophils secrete bioactive paucimannosidic proteins from azurophilic granules into pathogen-infected sputum. J Biol Chem *290*, 8789-8802. 10.1074/jbc.M114.631622.
13. Reiding, K.R., Lin, Y.H., van Alphen, F.P.J., Meijer, A.B., and Heck, A.J.R. (2021). Neutrophil azurophilic granule glycoproteins are distinctively decorated by atypical pauci- and phosphomannose glycans. Commun Biol *4*, 1012. 10.1038/s42003-021-02555-7.
14. Venkatakrishnan, V., Dieckmann, R., Loke, I., Tjondro, H.C., Chatterjee, S., Bylund, J., Thaysen-Andersen, M., Karlsson, N.G., and Karlsson-Bengtsson, A. (2020). Glycan analysis of human neutrophil granules implicates a maturation-dependent glycosylation machinery. J Biol Chem *295*, 12648-12660. 10.1074/jbc.RA120.014011.
15. Loke, I., Ostergaard, O., Heegaard, N.H.H., Packer, N.H., and Thaysen-Andersen, M. (2017). Paucimannose-Rich N-glycosylation of Spatiotemporally Regulated Human

Neutrophil Elastase Modulates Its Immune Functions. Mol Cell Proteomics *16*, 1507-1527. 10.1074/mcp.M116.066746.
16. Loke, I., Packer, N.H., and Thaysen-Andersen, M. (2015). Complementary LC-MS/MS-Based N-Glycan, N-Glycopeptide, and Intact N-Glycoprotein Profiling Reveals Unconventional Asn71-Glycosylation of Human Neutrophil Cathepsin G. Biomolecules *5*, 1832-1854. 10.3390/biom5031832.
17. Tjondro, H.C., Ugonotti, J., Kawahara, R., Chatterjee, S., Loke, I., Chen, S., Soltermann, F., Hinneburg, H., Parker, B.L., Venkatakrishnan, V., et al. (2021). Hyper-truncated Asn355- and Asn391-glycans modulate the activity of neutrophil granule myeloperoxidase. J Biol Chem *296*, 100144. 10.1074/jbc.RA120.016342.
18. Reiding, K.R., Franc, V., Huitema, M.G., Brouwer, E., Heeringa, P., and Heck, A.J.R. (2019). Neutrophil myeloperoxidase harbors distinct site-specific peculiarities in its glycosylation. J Biol Chem *294*, 20233-20245. 10.1074/jbc.RA119.011098.
19. Ugonotti, J., Kawahara, R., Loke, I., Zhu, Y., Chatterjee, S., Tjondro, H.C., Sumer-Bayraktar, Z., Neelamegham, S., and Thaysen-Andersen, M. (2022). N-acetyl-beta-D-hexosaminidases mediate the generation of paucimannosidic proteins via a putative noncanonical truncation pathway in human neutrophils. Glycobiology *32*, 218-229. 10.1093/glycob/cwab108.
20. Loke, I., Kolarich, D., Packer, N.H., and Thaysen-Andersen, M. (2016). Emerging roles of protein mannosylation in inflammation and infection. Mol Aspects Med *51*, 31-55. 10.1016/j.mam.2016.04.004.
21. Tjondro, H.C., Loke, I., Chatterjee, S., and Thaysen-Andersen, M. (2019). Human protein paucimannosylation: cues from the eukaryotic kingdoms. Biol Rev Camb Philos Soc *94*, 2068-2100. 10.1111/brv.12548.
22. Grabowski, P., Hesse, S., Hollizeck, S., Rohlfs, M., Behrends, U., Sherkat, R., Tamary, H., Unal, E., Somech, R., Patiroglu, T., et al. (2019). Proteome Analysis of Human Neutrophil Granulocytes From Patients With Monogenic Disease Using Data-independent Acquisition. Mol Cell Proteomics *18*, 760-772. 10.1074/mcp.RA118.001141.
23. Rieckmann, J.C., Geiger, R., Hornburg, D., Wolf, T., Kveler, K., Jarrossay, D., Sallusto, F., Shen-Orr, S.S., Lanzavecchia, A., Mann, M., and Meissner, F. (2017). Social network architecture of human immune cells unveiled by quantitative proteomics. Nat Immunol *18*, 583-593. 10.1038/ni.3693.
24. Parker, B.L., Thaysen-Andersen, M., Fazakerley, D.J., Holliday, M., Packer, N.H., and James, D.E. (2016). Terminal Galactosylation and Sialylation Switching on Membrane Glycoproteins upon TNF-Alpha-Induced Insulin Resistance in Adipocytes. Mol Cell Proteomics *15*, 141-153. 10.1074/mcp.M115.054221.
25. Kawahara, R., Recuero, S., Srougi, M., Leite, K.R.M., Thaysen-Andersen, M., and Palmisano, G. (2021). The Complexity and Dynamics of the Tissue Glycoproteome Associated With Prostate Cancer Progression. Mol Cell Proteomics *20*, 100026. 10.1074/mcp.RA120.002320.
26. Grassi, L., Pourfarzad, F., Ullrich, S., Merkel, A., Were, F., Carrillo-de-Santa-Pau, E., Yi, G., Hiemstra, I.H., Tool, A.T.J., Mul, E., et al. (2018). Dynamics of Transcription Regulation in Human Bone Marrow Myeloid Differentiation to Mature Blood Neutrophils. Cell Rep *24*, 2784-2794. 10.1016/j.celrep.2018.08.018.
27. Hoogendijk, A.J., Pourfarzad, F., Aarts, C.E.M., Tool, A.T.J., Hiemstra, I.H., Grassi, L., Frontini, M., Meijer, A.B., van den Biggelaar, M., and Kuijpers, T.W. (2019). Dynamic Transcriptome-Proteome Correlation Networks Reveal Human Myeloid Differentiation and Neutrophil-Specific Programming. Cell Rep *29*, 2505-2519 e2504. 10.1016/j.celrep.2019.10.082.

28. Borregaard, N., Heiple, J.M., Simons, E.R., and Clark, R.A. (1983). Subcellular localization of the b-cytochrome component of the human neutrophil microbicidal oxidase: translocation during activation. J Cell Biol *97*, 52-61. 10.1083/jcb.97.1.52.
29. Kawahara, R., Chernykh, A., Alagesan, K., Bern, M., Cao, W., Chalkley, R.J., Cheng, K., Choo, M.S., Edwards, N., Goldman, R., et al. (2021). Community evaluation of glycoproteomics informatics solutions reveals high-performance search strategies for serum glycopeptide analysis. Nat Methods *18*, 1304-1316. 10.1038/s41592-021-01309-x.
30. Rosales, C. (2020). Neutrophils at the crossroads of innate and adaptive immunity. J Leukoc Biol *108*, 377-396. 10.1002/JLB.4MIR0220-574RR.
31. Kaplan, M.J. (2013). Role of neutrophils in systemic autoimmune diseases. Arthritis Res Ther *15*, 219. 10.1186/ar4325.
32. Sonego, F., Castanheira, F.V., Ferreira, R.G., Kanashiro, A., Leite, C.A., Nascimento, D.C., Colon, D.F., Borges Vde, F., Alves-Filho, J.C., and Cunha, F.Q. (2016). Paradoxical Roles of the Neutrophil in Sepsis: Protective and Deleterious. Front Immunol *7*, 155. 10.3389/fimmu.2016.00155.
33. Garcia, R.C., Peterson, C.G., Segal, A.W., and Venge, P. (1985). Elastase in the different primary granules of the human neutrophil. Biochem Biophys Res Commun *132*, 1130-1136. 10.1016/0006-291x(85)91924-2.
34. Stavenhagen, K., Laan, L.C., Gao, C., Mehta, A.Y., Heimburg-Molinaro, J., Glickman, J.N., van Die, I., and Cummings, R.D. (2021). Tumor cells express pauci- and oligomannosidic N-glycans in glycoproteins recognized by the mannose receptor (CD206). Cell Mol Life Sci *78*, 5569-5585. 10.1007/s00018-021-03863-1.
35. Shepherd, V.L., and Hoidal, J.R. (1990). Clearance of neutrophil-derived myeloperoxidase by the macrophage mannose receptor. Am J Respir Cell Mol Biol *2*, 335-340. 10.1165/ajrcmb/2.4.335.
36. Gong, T., Liu, L., Jiang, W., and Zhou, R. (2020). DAMP-sensing receptors in sterile inflammation and inflammatory diseases. Nat Rev Immunol *20*, 95-112. 10.1038/s41577-019-0215-7.
37. Graham, S.A., Antonopoulos, A., Hitchen, P.G., Haslam, S.M., Dell, A., Drickamer, K., and Taylor, M.E. (2011). Identification of neutrophil granule glycoproteins as Lewis(x)-containing ligands cleared by the scavenger receptor C-type lectin. J Biol Chem *286*, 24336-24349. 10.1074/jbc.M111.244772.
38. Rudd, P.M., Mattu, T.S., Masure, S., Bratt, T., Van den Steen, P.E., Wormald, M.R., Kuster, B., Harvey, D.J., Borregaard, N., Van Damme, J., et al. (1999). Glycosylation of natural human neutrophil gelatinase B and neutrophil gelatinase B-associated lipocalin. Biochemistry *38*, 13937-13950. 10.1021/bi991162e.
39. Wright, R.D., and Cooper, D. (2014). Glycobiology of leukocyte trafficking in inflammation. Glycobiology *24*, 1242-1251. 10.1093/glycob/cwu101.
40. Taylor, M.E., and Drickamer, K. (2019). Mammalian sugar-binding receptors: known functions and unexplored roles. FEBS J *286*, 1800-1814. 10.1111/febs.14759.
41. Weinbaum, D.L., Sullivan, J.A., and Mandell, G.L. (1980). Receptors for concanavalin A cluster at the front of polarized neutrophils. Nature *286*, 725-727. 10.1038/286725a0.
42. Cao, H., Mathur, A., Robertson, C., Antonopoulos, A., Henderson, S., Girard, L.P., Wong, J.H., Davie, A., Wright, S., Brewin, J., et al. (2022). Measurement of erythrocyte membrane mannoses to assess splenic function. Br J Haematol *198*, 155-164. 10.1111/bjh.18164.
43. Park, D., Brune, K.A., Mitra, A., Marusina, A.I., Maverakis, E., and Lebrilla, C.B. (2015). Characteristic Changes in Cell Surface Glycosylation Accompany Intestinal Epithelial Cell (IEC) Differentiation: High Mannose Structures Dominate the Cell

Surface Glycome of Undifferentiated Enterocytes. Mol Cell Proteomics *14*, 2910-2921. 10.1074/mcp.M115.053983.
44. Heindel, D.W., Koppolu, S., Zhang, Y., Kasper, B., Meche, L., Vaiana, C.A., Bissel, S.J., Carter, C.E., Kelvin, A.A., Elaish, M., et al. (2020). Glycomic analysis of host response reveals high mannose as a key mediator of influenza severity. Proc Natl Acad Sci U S A *117*, 26926-26935. 10.1073/pnas.2008203117.
45. Chatterjee, S., Ugonotti, J., Lee, L.Y., Everest-Dass, A., Kawahara, R., and Thaysen-Andersen, M. (2021). Trends in oligomannosylation and alpha1,2-mannosidase expression in human cancers. Oncotarget *12*, 2188-2205. 10.18632/oncotarget.28064.
46. Park, D.D., Phoomak, C., Xu, G., Olney, L.P., Tran, K.A., Park, S.S., Haigh, N.E., Luxardi, G., Lert-Itthiporn, W., Shimoda, M., et al. (2020). Metastasis of cholangiocarcinoma is promoted by extended high-mannose glycans. Proc Natl Acad Sci U S A *117*, 7633-7644. 10.1073/pnas.1916498117.
47. Kissel, T., Toes, R.E.M., Huizinga, T.W.J., and Wuhrer, M. (2023). Glycobiology of rheumatic diseases. Nat Rev Rheumatol *19*, 28-43. 10.1038/s41584-022-00867-4.
48. Mukherjee, S., Jankevics, A., Busch, F., Lubeck, M., Zou, Y., Kruppa, G., Heck, A.J.R., Scheltema, R.A., and Reiding, K.R. (2022). Oxonium Ion-Guided Optimization of Ion Mobility-Assisted Glycoproteomics on the timsTOF Pro. Mol Cell Proteomics, 100486. 10.1016/j.mcpro.2022.100486.
49. Goldblatt, J., Lawrenson, R.A., Muir, L., Dattani, S., Hoffland, A., Tsuchiya, T., Kanegasaki, S., Sriskandan, S., and Pease, J.E. (2019). A Requirement for Neutrophil Glycosaminoglycans in Chemokine:Receptor Interactions Is Revealed by the Streptococcal Protease SpyCEP. J Immunol *202*, 3246-3255. 10.4049/jimmunol.1801688.
50. Lee, S., Bowrin, K., Hamad, A.R., and Chakravarti, S. (2009). Extracellular matrix lumican deposited on the surface of neutrophils promotes migration by binding to beta2 integrin. J Biol Chem *284*, 23662-23669. 10.1074/jbc.M109.026229.
51. Zhang, T., de Waard, A.A., Wuhrer, M., and Spaapen, R.M. (2019). The Role of Glycosphingolipids in Immune Cell Functions. Front Immunol *10*, 90. 10.3389/fimmu.2019.00090.
52. Blazev, R., Ashwood, C., Abrahams, J.L., Chung, L.H., Francis, D., Yang, P., Watt, K.I., Qian, H., Quaife-Ryan, G.A., Hudson, J.E., et al. (2021). Integrated Glycoproteomics Identifies a Role of N-Glycosylation and Galectin-1 on Myogenesis and Muscle Development. Mol Cell Proteomics *20*, 100030. 10.1074/mcp.RA120.002166.
53. Kimura, K., Koizumi, T., Urasawa, T., Ohta, Y., Takakura, D., and Kawasaki, N. (2021). Glycoproteomic analysis of the changes in protein N-glycosylation during neuronal differentiation in human-induced pluripotent stem cells and derived neuronal cells. Sci Rep *11*, 11169. 10.1038/s41598-021-90102-z.
54. Ashwood, C., Waas, M., Weerasekera, R., and Gundry, R.L. (2020). Reference glycan structure libraries of primary human cardiomyocytes and pluripotent stem cell-derived cardiomyocytes reveal cell-type and culture stage-specific glycan phenotypes. J Mol Cell Cardiol *139*, 33-46. 10.1016/j.yjmcc.2019.12.012.
55. Thaysen-Andersen, M., and Packer, N.H. (2012). Site-specific glycoproteomics confirms that protein structure dictates formation of N-glycan type, core fucosylation and branching. Glycobiology *22*, 1440-1452. 10.1093/glycob/cws110.
56. Harada, Y., Ohkawa, Y., Kizuka, Y., and Taniguchi, N. (2019). Oligosaccharyltransferase: A Gatekeeper of Health and Tumor Progression. Int J Mol Sci *20*. 10.3390/ijms20236074.

57. Stevens, K.L.P., Black, A.L., Wells, K.M., Yeo, K.Y.B., Steuart, R.F.L., Stirling, C.J., Schulz, B.L., and Mousley, C.J. (2017). Diminished Ost3-dependent N-glycosylation of the BiP nucleotide exchange factor Sil1 is an adaptive response to reductive ER stress. Proc Natl Acad Sci U S A *114*, 12489-12494. 10.1073/pnas.1705641114.
58. Yang, Q., Hughes, T.A., Kelkar, A., Yu, X., Cheng, K., Park, S., Huang, W.C., Lovell, J.F., and Neelamegham, S. (2020). Inhibition of SARS-CoV-2 viral entry upon blocking N- and O-glycan elaboration. Elife *9*. 10.7554/eLife.61552.
59. King, S.L., Goth, C.K., Eckhard, U., Joshi, H.J., Haue, A.D., Vakhrushev, S.Y., Schjoldager, K.T., Overall, C.M., and Wandall, H.H. (2018). TAILS N-terminomics and proteomics reveal complex regulation of proteolytic cleavage by O-glycosylation. J Biol Chem *293*, 7629-7644. 10.1074/jbc.RA118.001978.
60. Malengier-Devlies, B., Metzemaekers, M., Wouters, C., Proost, P., and Matthys, P. (2021). Neutrophil Homeostasis and Emergency Granulopoiesis: The Example of Systemic Juvenile Idiopathic Arthritis. Front Immunol *12*, 766620. 10.3389/fimmu.2021.766620.
61. Manz, M.G., and Boettcher, S. (2014). Emergency granulopoiesis. Nat Rev Immunol *14*, 302-314. 10.1038/nri3660.
62. Mackey, J.B.G., Coffelt, S.B., and Carlin, L.M. (2019). Neutrophil Maturity in Cancer. Front Immunol *10*, 1912. 10.3389/fimmu.2019.01912.
63. Lukasova, E., Koristek, Z., Klabusay, M., Ondrej, V., Grigoryev, S., Bacikova, A., Rezacova, M., Falk, M., Vavrova, J., Kohutova, V., and Kozubek, S. (2013). Granulocyte maturation determines ability to release chromatin NETs and loss of DNA damage response; these properties are absent in immature AML granulocytes. Biochim Biophys Acta *1833*, 767-779. 10.1016/j.bbamcr.2012.12.012.
64. Jensen, P.H., Karlsson, N.G., Kolarich, D., and Packer, N.H. (2012). Structural analysis of N- and O-glycans released from glycoproteins. Nat Protoc *7*, 1299-1310. 10.1038/nprot.2012.063.
65. Ceroni, A., Maass, K., Geyer, H., Geyer, R., Dell, A., and Haslam, S.M. (2008). GlycoWorkbench: a tool for the computer-assisted annotation of mass spectra of glycans. J Proteome Res *7*, 1650-1659. 10.1021/pr7008252.
66. Everest-Dass, A.V., Kolarich, D., Campbell, M.P., and Packer, N.H. (2013). Tandem mass spectra of glycan substructures enable the multistage mass spectrometric identification of determinants on oligosaccharides. Rapid Commun Mass Spectrom *27*, 931-939. 10.1002/rcm.6527.
67. Adams, K.J., Pratt, B., Bose, N., Dubois, L.G., St John-Williams, L., Perrott, K.M., Ky, K., Kapahi, P., Sharma, V., MacCoss, M.J., et al. (2020). Skyline for Small Molecules: A Unifying Software Package for Quantitative Metabolomics. J Proteome Res *19*, 1447-1458. 10.1021/acs.jproteome.9b00640.
68. Ashwood, C., Lin, C.H., Thaysen-Andersen, M., and Packer, N.H. (2018). Discrimination of Isomers of Released N- and O-Glycans Using Diagnostic Product Ions in Negative Ion PGC-LC-ESI-MS/MS. J Am Soc Mass Spectrom *29*, 1194-1209. 10.1007/s13361-018-1932-z.
69. Cox, J., and Mann, M. (2008). MaxQuant enables high peptide identification rates, individualized p.p.b.-range mass accuracies and proteome-wide protein quantification. Nat Biotechnol *26*, 1367-1372. 10.1038/nbt.1511.
70. Cox, J., Hein, M.Y., Luber, C.A., Paron, I., Nagaraj, N., and Mann, M. (2014). Accurate proteome-wide label-free quantification by delayed normalization and maximal peptide ratio extraction, termed MaxLFQ. Mol Cell Proteomics *13*, 2513-2526. 10.1074/mcp.M113.031591.

71. Tyanova, S., Temu, T., Sinitcyn, P., Carlson, A., Hein, M.Y., Geiger, T., Mann, M., and Cox, J. (2016). The Perseus computational platform for comprehensive analysis of (prote)omics data. Nat Methods *13*, 731-740. 10.1038/nmeth.3901.
72. Xia, J., Psychogios, N., Young, N., and Wishart, D.S. (2009). MetaboAnalyst: a web server for metabolomic data analysis and interpretation. Nucleic Acids Res *37*, W652-660. 10.1093/nar/gkp356.